Adaptive modification of lipid droplets mediated by Plin1 functions in infection-induced pathogenesis in *Drosophila*

Lei Wang[1,2,5], Jiaxin Lin[2,3,5], Junjing Yu[4], Zhiqin Fan[2,3], Hong Tang[2 #] and Lei Pan[2,3,6 #]

[1] Wuhan Institute of Virology, Chinese Academy of Sciences, Wuhan, Hubei 430071, China

[2] Key Laboratory of Molecular Virology and Immunology, Institut Pasteur of Shanghai, Chinese Academy of Sciences, Shanghai 200031, China

[3] CAS Center for Excellence in Biotic Interactions, University of Chinese Academy of Sciences, Beijing 100049, China

[4] Shanghai Institute of Biochemistry and Cell Biology, Chinese Academy of Sciences, Shanghai 200031, China.

[5] University of Chinese Academy of Sciences, Beijing 100049, China

[6] Lead contact

#Correspondence: H. Tang (htang@ips.ac.cn) or L. Pan (panlei@ips.ac.cn).

ABSTRACT

Lipid droplets（LDs）are important intracellular dynamic organelles for lipid metabolism. However, the relationship between the status of LDs and innate immune response to infection, especially the underlying mechanisms remain largely unknown. Herein, we describe the morphological dynamic of LDs in fat body of *Drosophila*, which is different between transient and sustained bacterial infection. Detailed analysis shows that *perilipin1* (*plin1*), a core gene regulating lipid metabolism of LDs, is suppressed by innate immune signaling, IMD/Relish pathway, via Martik (MRT) /Putzig (PZG) complex. In transient immune activation, downregulated *plin1* promotes the formation of large LDs, which alleviates immune reactions-induced reactive oxygen species (ROS) stress. Thereby, the growth of LDs is likely an active adaptation in response to IMD activation, which maintains redox homeostasis. Whereas in sustained inflammatory condition, *plin1* deficiency accelerates excessive decomposition of large LDs through recruitment of Brummer/ATGL lipase on LDs, which results in energy wasting and severe lipotoxicity, thus deteriorated pathogenesis. Taken together, our study provides evidences that *plin1* has dual function on LDs' morphology to regulate infection-induced pathogenesis, and Plin1 might be a potential therapeutic target for coordinating the resolution of inflammation and lipid metabolism in LDs.

INTRODUCTION

Immune activation is always tightly accompanied with metabolic reprogramming, which redistributes energy consumption to guarantee the priority of immune protection against pathogenic infection (Hotamisligil, 2017; O'Neill et al., 2016). Thereby, the

homeostatic regulation of metabolism in response to immunoreaction is critical for the host fitness. Unlike transient infection, sustained infection is often associated with chronic pathogenesis, which subsequently results in metabolic disorders, the main threat to the individual health. Besides carbohydrate metabolism, lipid provides another important bioenergetic and synthetic resources *in vivo*. Quite a few of lipid metabolites have been reported to play roles in pro-inflammation or anti-inflammation (Arita, 2012; Serhan et al., 2014; Walpole GFW, 2018). However, the dynamics and differences of lipid metabolism in transient and sustained inflammatory conditions are barely described so far.

Lipid droplets（LDs）are important intracellular organelles in all eukaryotic and some prokaryotic cells(Murphy, 2001), providing the major place for lipid synthesis, lysis, transfer and storage. These organelles contain a phospholipid monolayer surrounding neutral lipids, such as di/triacylglycerols or sterol esters (Tauchi-Sato et al., 2002). Because LDs function mainly through storing and providing energy(Walther and Farese, 2012), they appear to be involved in multiple physiological and pathological processes in the host. The emerging evidences have shown that LDs are responsive to ER stress(Fu et al., 2011), buffer starvation stimulation(Velazquez et al., 2016) , play roles in diseases, such as diabetes and cancer(Cohen JC, 2011; Greenberg et al., 2011). Most intriguingly, LDs also take participate in immune regulation including but not limit to modulating functions of myeloid cells (den Brok et al., 2018), combating pathogenic bacterial infection, exploited by virus and so on (Saka and Valdivia, 2012; Vallochi et

68 al., 2018; Welte, 2015). The number, size and anchored proteins of LDs are dynamically
69 changing during the period of infection or inflammation (Harsh et al., 2019; Henne et
70 al., 2018; Menon et al., 2019). So that this diversification makes it difficult for LDs to
71 be viewed as either pro-inflammatory or anti-inflammatory modulators(Pereira-Dutra
72 et al., 2019). It strongly indicates that the homeostasis of LDs should be tightly
73 controlled. Defects in the biogenesis and the mobilization of LDs will result in free fatty
74 acid induced lipotoxicity(Ertunc and Hotamisligil, 2016; Listenberger et al., 2003) or
75 even the accumulation of pro-inflammatory mediators(Feldstein et al., 2004; Summers,
76 2006), all of which lead to metaflammation accompanied with organelles dysfunction,
77 secondary inflammatory responses and exacerbated dysbiosis of metabolism(Ertunc
78 and Hotamisligil, 2016). However, the role and dynamic pattern of LDs during immune
79 activation still remain obscure. Especially, the factors mediating this immunometabolic
80 switches of LDs have not been well identified.
81
82 *Drosophila melanogaster* has emerged as a productive organism to investigate
83 immunometabolism, due to the advantages of powerful genetic manipulation and
84 highly conserved mechanisms in both innate immunity and metabolism (Heier and
85 Kuhnlein, 2018; Lemaitre and Hoffmann, 2007; Myllymaki et al., 2014). Especially,
86 the fat body (analogous to human liver and adipose tissue) is an ideal place for studying
87 the interaction between LDs' metabolism and inflammation, which thanks to its
88 richness of LDs and its role as a major organ mediating systemic innate
89 immunity(Arrese and Soulages, 2010; Kleino and Silverman, 2014). LDs are not

homogenous organelles, which accommodates hundreds of variable proteins (Beller M et al., 2006; Guo Y et al., 2008). However, Perilipins (Plins) are important constitutive proteins on the surface of LDs (Itabe et al., 2017; Kimmel and Sztalryd, 2016). There are two Plins in *Drosophila*, Lipid storage droplet-1 (*lsd1*, homologous to human PLIN1) and *lsd2* (homologous to human PLIN2) (Bickel et al., 2009). *plin2* acts to promote lipid storage and LDs' growth as a barrier for lipase(Fauny et al., 2005; Grönke et al., 2003; Teixeira et al., 2003), while *plin1* modulates protein flux on LDs(Beller et al., 2010; Bi et al., 2012). In human or mouse adipocyte tissue, PLIN1 deficiency led to inflammatory cells infiltration and uncontrollable LDs lipolysis (Gandotra S, 2011; Sohn et al., 2018; Tansey et al., 2001). Depletion of infiltrated immune cells or inhibition of lipase, adipose triglyceride lipase (ATGL) or hormone-sensitive lipase (HSL), alleviated this metaflammation(Cani et al., 2007; Schweiger et al., 2017), which indicates a link between PLIN1 controlled LDs and immunometabolism. However, the function of LDs and underlying mechanisms involving Plins in response to infection are still poorly understood.

In this study, the dynamic switches in morphology and number of LDs during transient and sustained inflammation, induced either by bacterial infection or genetic manipulation, were compared. Plin1 was found to have a dual function to regulate LDs' morphology in different inflammatory conditions. And adaptive modification of LDs acts as a potential modulator of infection-induced pathogenesis.

Results

113 **Immune activation modulates lipid metabolism, particular the morphology of**
114 **lipid droplets (LDs) in the fat body**.
115 In *Drosophila*, the fat body is not only a center organ mediating systemic immune
116 responses, but also the major place for lipid metabolism. Thus, to decipher the
117 mechanistic connections between innate immunity and lipid metabolism, triglycerides
118 (TAGs) kinetics was detected in the fat body of *Drosophila* after systemic infection.
119 Two bacteria were applied to perform nano-injection to infect adult fruit flies. One
120 bacterium is a fly non-pathogenic Gram-negative bacterium, *Escherichia. Coli* (*E. coli*),
121 which infection results in a transient innate immune response within 48 hour post
122 infection (hpi)(Vodovar et al., 2005). The other one is a fly deadly pathogenic Gram-
123 negative bacterium, *Salmonella. Typhimurium* (*S. typhimurium*), which causes a
124 sustained intracellular infection that triggers a prolonged inflammatory responses in
125 *Drosophila*(Brandt et al., 2004). The immune deficiency (IMD) pathway is the
126 dominant innate immune singling against Gram-negative bacterial infection, which
127 regulates Relish/NF-κB-dependent transcription of AMPs, such as *Diptericin* (*Dpt*)
128 (Hoffmann JA., 2003; JA., 2003; Kaneko T, 2004; Lemaitre and Hoffmann, 2007;
129 Lemaitre, 2007). Therefore, measuring the expression level of *Dpt* can monitor the IMD
130 signaling activity in turn (Leulier et al., 2003; Neyen et al., 2016). Infection by both
131 bacteria led to a gradient increase of IMD activity in the fat body from 0 hpi to 12 hpi.
132 However, the transient immune response induced by *E. coli* infection subsided to the
133 basal level after 48 hpi (**Fig.1A**), until then the prolonged activation of IMD still
134 continuously increased after *Salmonella* infection (**Fig. 1B**). Interestingly, compared

135 with mock injection control (**Supplementary Fig. S1A**), the TAGs level in the fat body
136 of flies with *E.coli* infection steadily increased from 6 hpi to 16 hpi, then a decline at
137 24 hpi and almost recovered after 48 hpi (**Fig. 1A**). But after *S. typhimurium* infection,
138 the TAGs level presented a continuous decrease in the fat body, which was in negative
139 correlation with progressively increased IMD activity (**Fig. 1B**). Moreover, only a
140 decrease of TAGs level was observed in the whole body after *E.coli* infection
141 (**Supplementary Fig. S1B**), which suggested a preferred lipid import rather than *de*
142 *novo* fatty acid synthesis in the fat body from 0 hpi to 12 hpi. It is also consistent with
143 previous studies that the transcriptional levels of the most triglyceride synthesis genes
144 are suppressed in the beginning period of infection (Clark et al., 2013; Dionne et al.,
145 2006). While in the case of sustained infection by *S. typhimurium,* the TAGs level was
146 continuously decreased in the whole body (**Supplementary Fig. 1C**) as that in the fat
147 body (**Fig. 1B**). However, these results indicated a link between lipid metabolism and
148 IMD signaling activation.
149
150 LDs is the major place for lipid anabolism, catabolism and mobilization(Kühnlein,
151 2012), which prompted us to investigate whether the morphology of LDs in the fat body
152 responds to bacterial infection. Compared with PBS injection group (**Fig. 1C and 1C1**),
153 BODIPY staining cells of fat bodies showed that both *E. coli* and *S. typhimurium*
154 infection increased the percentage of intracellular small LDs (diameter < 2 μm) at 6 hpi
155 (**Fig. 1C and 1C2- C3**). Then, LDs trended to become bigger at 16 hpi indicated by the
156 decrease of small LDs percentage and the increase of large LDs (diameter > 4 μm)

157 percentage, and then this size distribution of LDs was restoring to the basal level at 24
158 h post *E. coli* infection (**Fig. 1*C* and 1*C*2**), while the percentage of small LDs kept on
159 increasing after *S. typhimurium* infection (**Fig. 1*C* and 1*C*3**). Similar to the changes of
160 TAGs level, the average size of LDs in fat body cells raised up before 16 h and
161 decreased at 24 h post *E. coli* infection, which of that was only continuous decreasing
162 after *S. typhimurium* infection (**Supplementary Fig. S1D**). These results indicated that
163 small LDs were firstly prone to fuse into bigger ones within 16 h of *E. coli* infection.
164 On the contrary, large LDs tended to decompose during *S. typhimurium* infection (**Fig.**
165 **1*C* and Supplementary Fig. S1D**). Therefore, these results suggested that the
166 morphology of LDs in the fat body changed according to bacterial infection, but
167 different in transient and sustained infectious condition.
168
169 **IMD signaling activation sufficiently modifies the morphology of LD.**
170 To determine whether the IMD activation rather than the potential bacterial effects is
171 responsible for the modification of LDs during infection, a fat body-specific RU486-
172 inducible GAL4 driver (*GS106-GAL4*) (Roman et al., 2001) was applied to detect the
173 relationship between IMD signaling and LDs' patterns in the fat body. Ectopic
174 expression of either different isoforms of *PGRP-LC* (*PGRP-LCx* or *PGRP-LCa*), the
175 receptor of IMD signaling pathway (Choe et al., 2002; He et al., 2017; Yang et al., 2019),
176 or the N-terminal of *Relish* (*Rel.68*), the *Drosophila* NF-kB factor (Wiklund et al.,
177 2009), resulted in a constitutive activation of IMD signaling (**Supplementary Fig.**
178 **S1E-G**). IMD activation by *GS106-GAL4* in fat bodies caused an increase of TAGs
179 level in the fat body at 12 h after RU486 treatment (**Fig. 1D and 1E**), simultaneously,

180 the TAGs level of whole body didn't change within 12 hpi (**Supplementary Fig. S1H-**
181 **I**). These results recalled the phenotypes in the early stage (within 12 hours) of transient
182 infection by *E. coli*. However, this elevation of TAGs level in fat bodies of WT flies
183 disappeared in that of flies with mutation along IMD signaling pathway (*imd*^{1}、*PGRP-*
184 *LC*$^{\Delta 5}$ and *relish*^{E20}) at 12h post injection with heat-killed *E. coli* (These immune
185 deficient flies died too quickly when primed by live bacteria.) (**Fig. 1F and**
186 **Supplementary Fig. S1J**). Furthermore, IMD signaling deficiency also hampered the
187 increase of LDs size at 16 hpi, comparing with WT control (**Supplementary Fig. S1K-**
188 **L**). Whereas, prolonged hyper-activation of IMD signaling induced by RU486 (after
189 24 hpi) led to a dramatic decrease of TAGs level in both fat body and the whole body
190 (**Fig. 1D-E and Supplementary Fig. S1H-I**), accompanying with the decrease of both
191 the percentage of large LDs (**Fig. 1G and 1G1-G3**) and the average LDs size in the fat
192 body (**Fig. 1H**), all of which was reminiscent of that in sustained infection by *S.*
193 *typhimurium*. Therefore, these results suggested IMD activation is necessary and
194 enough to modify LDs.
195
196 ***plin1* is involved in LDs modification induced by IMD activation.**
197 To explore the underlying mechanisms of LD's metabolism in response to immune
198 activation, genes involved in the regulation of LDs (Beller et al., 2010; Grönke et al.,
199 2003; Heier and Kuhnlein, 2018; Kühnlein, 2012) were tested in fat bodies by real-time
200 PCR. After comprehensive analysis of mRNA expression, only four genes, *APGAT2,*
201 *DGAT2, Rfabg* and *plin1*, showed opposite transcriptional trends (from 4 hpi to 12 hpi)
202 in transient infection by *E. coli* when comparing with sustained infection by *S.*

203 *typhimurium* (**Supplementary Fig. S2*A* and S2*B***). Further, we noticed that the
204 expression level of *plin1* present the most reduction in the fat body, in which IMD
205 overactivated through overexpressing *Rel.68* by fat body-specific driver *ppl-GAL4*
206 (**Supplementary Fig. S2*C***). Therefore, these results indicated a potential role of *plin1*
207 in the regulation of LD's metabolism accompanied with IMD activation.
208
209 Interestingly, reminiscent of the correlation between TAGs level and IMD activity in
210 the fat body during bacterial infection of flies (**Fig. 1A**), transient infection by *E. coli*
211 induced a significant downregulation of the mRNA level of *plin1* at 4 hpi, which was
212 then restored to the basal level at 24 hpi (**Fig. 2A**). While prolonged overactivation of
213 IMD signaling either by sustained intracellular *S. typhimurium* infection (**Fig. 2B**), or
214 by RU486 treatment in fat body-specific GS flies (**Fig. 2C**), led to continuous reduced
215 *plin1* expression. Martik (MRT) /Putzig (PZG) complex, a chromosome remodeling
216 complex, was reported to suppress *plin1* at transcriptional level (Yao et al., 2018).
217 Intriguingly, both mRNA levels of *mrt* and *pzg* rose up in the fat body after bacterial
218 infection (**Fig. 2D and Supplementary Fig. S3A**). Noteworthily, homologous
219 alignment showed that at least one conserved binding motif of Relish existed in the
220 promoter region of both *mrt* and *pzg* genes across *Drosophila* species with different
221 evolutionary ages (**Supplementary Fig. S3B and S3C)**. It implied a potential
222 regulation of Relish on these genes. Peptidoglycan (PGN) derived from gram-negative
223 bacteria can activate IMD signaling in *Drosophila* S2* cells *in vitro* (Kaneko T, 2004).
224 Indeed, the luciferase activity controlled by the promoter of *mrt* or *pzg* was significantly

225 enhanced in S2* cells after PGN treatment, which was blocked by the knockdown of
226 Relish using dsRNA (He et al., 2017) (**Fig. 2E and Supplementary Fig. S3D**).
227 Additionally, two Relish binding motifs flanked truncated *mrt* promoter region (T-
228 *mrt(RelB)*, -870 to +1bp) were critical for *mrt* transcription (**Fig. 2F and**
229 **Supplementary Fig. S3E**), because PGN treatment didn't enhance T-*mrt*-Luc activity
230 any more when these two sites were removed (**Fig. 2F**). Thus, these results suggested
231 the suppression of *plin1* by IMD signaling might be through upregulation of mrt/pzg.
232 In consistent with previous studies (Beller et al., 2010; Bi et al., 2012), *plin1* deficiency
233 by mutation (*plin1*^{38}) or fat body specific knockdown (*UAS-plin1 RNAi* driven by *ppl-*
234 *GAL4*) promoted the formation of large LDs (**Fig. 2G)**. In contrast, ectopic expression
235 of *plin1* in fat bodies enhanced lipid mobilization and inhibited LD coalescence (Yao
236 et al., 2018), thus led to the accumulation of small LDs (**Fig. 2G**). All together, these
237 results provided explanation for LDs' growth in the early stage of transient IMD
238 activation.
239

240 **Sustained immune activation prefers to accelerate lipolysis of large LDs in a**
241 **Bmm/ATGL-dependent manner.**

242 However, unlike transient IMD activation promoted LDs' growth (**Fig. 1C and**
243 **Supplementary Fig. S1D**), sustained IMD hyper-activation in the fat body, either
244 driven by *ppl-GAL4* **(Fig. 3A)** or RU486 inducible *GS106-GAL4* for 5 days **(Fig. 3B**
245 **and 3B1)**, instead accelerated large LDs decomposition and small LDs generation.
246 Simultaneous deficiency **(Fig. 3A)** or knockdown **(Fig. 3B)** of *plin1* in the fat body

247 induced the formation of large LDs **(Fig. 3B1)**, with note that the average size of these
248 LDs is smaller than that of flies with *plin1* deficiency alone **(Fig 2G)**, but bigger than
249 that of RU486-untreated controls(**Fig. 3B** and **3B1**). Although these results confirmed
250 the function of Plin1 in reducing LDs' growth, it is worthy to explore mechanism why
251 IMD-induced autonomous downregulation of *plin1* was unable to overcome LDs'
252 breakdown in prolonged immune activation condition. Thus, the long time-course of
253 LDs' morphological change was traced in the fat body of flies with IMD overactivation
254 (*ppl-Gal4>Rel.68*). Although *plin1* deficiency made *ppl-Gal4>Rel.68;plin1*^{38} flies
255 have much larger LDs than that of *ppl-gal4>Rel.68* at the first week after eclosion,
256 these larger LDs then experienced much faster decomposition rate (**Fig. 3C**).
257 Intriguingly, no matter the distribution of LDs size (**Fig. 3C1-C2**) or the average LDs
258 size (**Fig. 3D**) had no significant differences in the fat body of *ppl-GAL4>Rel.68* and
259 *ppl-GAL4>Rel68;plin1*^{38} flies since the second week. Therefore, these results
260 suggested that decomposition of LDs occurred quickly and preferred on large LDs
261 during sustained immune activation.
262
263 Persistent inflammation always over-consumes energy, most of which is provided by
264 lipolysis. Indeed, sustained IMD activation in the fat body (*ppl-GAL4>Rel.68*)
265 enhanced the decrease of TAGs level in the whole body, very interestingly, which
266 became much faster when removing *plin1* simultaneously (*ppl-GAL4>Rel68;plin1*^{38})
267 (**Supplementary Fig. S4A**). For further confirmation, these flies were treated with
268 nutrient starvation, a much more sensitive condition. *plin1* mutation indeed

269 dramatically enhanced TAGs consumption rate in *ppl-GAL4>Rel.68;plin1*^{38} flies since
270 the start of starvation, comparing with *ppl-GAL4>Rel.68* flies (**Fig. 3E**). Consequently,
271 flies with a higher TAGs consumption rate were more sensitive to starvation (**Fig. 3F**).
272 Previous study suggested that LDs lipolysis predominately mediated by Brummer
273 (Bmm), the *Drosophila* homolog of mammalian adipose TAG lipase (ATGL)(Grönke
274 S, 2007; Gronke et al., 2005). Fat body-specific knockdown of *Bmm* effectively blocked
275 the quick decomposition of large LDs in the fat body of both *ppl-GAL4>Rel.68* and
276 *ppl-GAL4>Rel68;plin1*^{38} flies (**Fig. 3G**), and even further promoted the LDs growth in
277 the fat body (**Fig. 3H)** as well as TAGs content of the whole body **(Supplementary**
278 **Fig. S4B**). Furthermore, *Bmm-GFP* knock-in allele was applied to detect the
279 localization of Bmm on LDs under normal and IMD-activated condition. Compared
280 with control, IMD activation by fat body-specific overexpression of *Rel.68* significantly
281 enhanced the Bmm-GFP abundance on the surface of LDs. It's worthy to note that
282 Bmm-GFP signals were largely concentrated in the contact site between LDs, a sign of
283 overactive lipolysis (Gronke et al., 2005) (**Fig. 3I**). Together, these results suggested
284 that sustained IMD activation enhanced Bmm/ATGL-mediated lipolysis of large LDs.
285
286 ***plin1* compromises host protection against bacterial infection**.
287 Naturally, whether *plin1*-mediated LDs modification participated in the regulation of
288 immune function was detected next. Compared with genetic controls, either *plin1*
289 deficiency (*plin1*^{38}) (**Fig. 4A and 4B**) or fat body-specific knockdown of *plin1* (*ppl-*
290 *GAL4>UAS-plni1RNAi*) (**Fig. 4C and 4D**) prolonged the survival rate and reduced
291 bacterial loads (colony-forming units, CFUs) after *S. typhimurium* systemic infection,

292 indicative of enhanced resistance against bacterial infection. Conversely, ectopic
293 expression of *plin1* in the fat body (*ppl-GAL4>UAS-plin1*) led to a dramatic increase
294 of mortality rate of flies infected by *S. typhimurium* (**Fig. 4E ,** Reducing infection OD
295 because O.E.*plin1* flies died too quickly.**)**, and even by non-pathogenic *E. coli* (**Fig.**
296 **4G)**, likely due to uncontrolled bacterial growth **(Fig. 4F and 4H**). To exclude the
297 potential effects of *plin1* on flies' development, RU486 induced fat body-specific GAL4
298 (*GS106-GAL4*) was used after fly eclosion. After RU486 treatment for 3 days, the
299 significant decrease or increase of LDs size by overexpression or knockdown of *plin1*,
300 respectively, was clearly observed in the fat body (**Fig. 4I**). Since then, flies were
301 challenged with *S. typhimurium*. As expected, downregulation of *plin1* prolonged the
302 survival rate, while upregulation of *plin1* shortened the survival rate and elevated
303 bacterial loads after *S. typhimurium* infection (**Fig. 4J and 4K**). However, deficiency
304 of *plin1* did not affect anti-microbial peptides (AMPs) (*Diptericin*, *Dpt; AttacinA, AttA*)
305 response upon *E. coli* infection (**Supplementary Fig. S5A**), but particularly improved
306 *Dpt* expression upon *S. typhimurium* infection (**Supplementary Fig. S5B**). More
307 interestingly, overexpression of *plin1* obviously dampened the AMPs response in both
308 *E. coli* and *S. typhimurium* infection (**Supplementary Fig. S5C and S5D**). Taken
309 together, these results suggested that adaptive downregulation of *plin1* in response to
310 IMD signaling activation at least benefited the host against bacterial infection.
311
312 **Large LDs relieves oxidative stress associated with immune activation.**
313 Lipid metabolic disorder usually follows sustained inflammation response. And one
314 hallmark is excessive lipolysis-induced lipotoxicity (Blaser et al., 2016; Grisouard et

315 al., 2012; Morgan and Liu, 2011; Zu et al., 2009), which is one causative factor for
316 reactive oxidative species (ROS)-related tissue damages(Ertunc and Hotamisligil, 2016;
317 Herms et al., 2013; Listenberger et al., 2003). Since LDs are major hubs for lipid
318 metabolism in fat body cells, it promoted us to investigate whether *plin1*-mediated LDs
319 modification during immune response regulates intracellular redox homeostasis. A
320 transgenic allele with a *gstD-GFP* insertion was applied to monitor ROS activity *in vivo*
321 by measuring GFP intensity (Sykiotis and Bohmann, 2008). Transient infection by
322 *E.coli* only induced a slight and temporary elevation of ROS level in the fat body at 16
323 hpi. However, *S. typhimurium* infection resulted in a continuous and strong increase of
324 intracellular ROS level in fat bodies (**Fig. 5A and 5A1-A2**). Additionally, fluorescent
325 probe 2',7'-dichlorofluorescein diacetate (DCFH-DA) was also used to evaluate
326 intracellular ROS level. DCFH-DA staining showed that sustained IMD activation
327 induced by RU486 feeding for 5 days caused a significant increase of ROS levels in the
328 fat body of *GS106-GAL4>PGRP-LC* (*LCa or LCx*) and *GS106-GAL4>Rel.68* flies (**Fig.**
329 **5B and 5B1-B3**). These results suggested a link between sustained IMD activation and
330 accumulated intracellular oxidative stress. To determine whether immune activation
331 induced-oxidative stress affects the host against bacterial infection, N-acetylcysteine
332 (NAC), a widely-used ROS scavenger, was fed to flies after *S. typhimurium* infection.
333 Feeding flies with NAC at 12 h, not 0h, post *S. typhimurium* infection, just when the
334 excessive ROS accumulation was already rapidly developing (**Fig. 5A**), significantly
335 improved flies' survival, compared to non-feeding control (**Fig. 5C**). These results
336 suggested that oxidative stress developing with sustained immune response is harmful

337 to fly after bacterial infection.

338

339 Very impressively, data correlation analysis showed that there seemed to be a positive
340 correlation between the continuously increased percentage of small LDs (< 2 μm) and
341 the gradient accumulated ROS intensity in fat body cells after *S. typhimurium* infection
342 (**Fig. 5D**). Recalling the phenotypes of low ROS intensity and large LDs formation in
343 WT flies during transient infection by *E. coli* (**Fig. 5A and Fig. 1C**), whether large LDs
344 has ability against intracellular oxidative stress was determined next. *plin1* deficiency
345 (*plin1*^{38}) or knockdown (*UAS-plin1RNAi* driven by *ppl-GAL4*), which promoted LDs
346 growth, contained the lower level of ROS than that of control (**Fig. 5E and 5E1-E2**).
347 In contrast, overexpressing *plin1*（*ppl-GAL4> plin1*）, which transformed LDs into
348 smaller ones, led to a much higher level of ROS intensity (**Fig. 5E and 5E2**). The
349 similar phenotypes were observed in fat body-specific *GS106-GAL4* flies after RU486
350 induction (**Fig. 5F and 5F1-F2).** Intriguingly, further removing *plin1* from *ppl-*
351 *GAL4>Rel.68* flies significantly ameliorated ROS accumulation in the fat body in this
352 sustained IMD activated condition (**Fig. 5G and 5G1**). More importantly, deficiency
353 of *plin1* significantly prolonged the survival rate of *ppl-GAL4>UAS-Rel.68* flies after
354 *S. typhimurium* infection, with the note that flies with IMD hyper-activation alone (*ppl-*
355 *GAL4>UAS-Rel.68*) were more susceptible to *S. typhimurium* infection than its genetic
356 control (**Fig. 5H**). In addition, if we blocked the decomposition of large LDs associated
357 with IMD overactivation by knockdown of *Bmm* in the fat body, it strikingly benefited
358 the survival of *ppl-GAL4>Rel.68* flies as well, even without infection (**Fig. 5I**).

359 Therefore, these results suggested that large LDs formation contributed to alleviate the
360 intracellular oxidative stress induced by IMD activation. And Plin1 might serve as an
361 important linker to respond to IMD signaling and to modify LDs.
362
363 To further investigate antioxidative role of LDs, the morphology of LDs in fat body
364 cells was examined in flies with disruption of ROS metabolism. In *Drosophila*,
365 superoxide dismutase genes (*sod1/sod2*) or catalase gene (*cat*) encoded enzymes for
366 intracellular ROS clearance (C M Griswold et al., 1993; J P Phillips et al., 1989).
367 Knockdown of either *sod1*, *sod2* or *cat*, which led to excessive ROS accumulation,
368 promoted LDs growth significantly (**Fig. 6A and 6B**). Interestingly, once these flies
369 were fed with NAC to remove intracellular ROS, the morphology and the average size
370 of LDs almost reverted to the level as controls (**Fig. 6A and 6B**). Furthermore,
371 simultaneously overexpressing *plin1* or *Bmm* in the fat body sufficiently blocked the
372 formation of large LDs in *ppl-GAL4>UAS-sod1-RNAi*, *sod2-RNAi* or *cat-RNAi* flies
373 (**Fig. 6C and 6D**), which as expect caused much stronger ROS accumulation than
374 controls (**Fig. 6E and 6F**). Taken together, these results suggested that adaptive LDs
375 growth benefited flies to resist oxidative stress.
376
377
378 **Discussion**
379 Lipid metabolic reprogramming has been widely reported to associate with immune
380 responses (Buck et al., 2017; Hotamisligil, 2017; O'Neill et al., 2016). As the major
381 intracellular organelle for lipid metabolism and storage, LDs also seem to be involved

382 in immune process. Immune stimulation either by infection with bacteria (D'Avila et
383 al., 2006; Peyron et al., 2008), virus (Barba G, 1997; Hope et al., 2002; Samsa et al.,
384 2009), fungus(Sorgi et al., 2009) and protozoan parasites (Vallochi et al., 2018), or by
385 inoculation with cytokines(Bandeira-Melo et al., 2001; Pacheco P et al., 2002) is able
386 to promote the biogenesis of LDs in mammalian leukocytes. Recently, Hash et al also
387 confirmed that LDs are infection-inducible organelles in the gut of *Drosophila* at a
388 certain timepoint after infection (Harsh et al., 2019). However, the status and
389 morphology of LDs is changing rapidly *in vivo*. The dynamic transformation of LDs
390 during immune response, and in turn whether LDs status link to the regulation of
391 pathogenesis is rarely described.
392
393 In our study (**Fig.7**), we carefully traced the time-course morphogenesis of LDs in the
394 fat body beside the dynamic curve of IMD signaling activity. We found that transient
395 IMD activation (within 12hpi) by non-pathogenic bacterial infection promoted LDs'
396 growth in the fat body. The LDs' size and TAGs level in the fat body peaked when IMD
397 activity achieved its peak. However, the TAGs level in the whole body decreased
398 around that period, suggesting the substrates for LDs' biogenesis in the fat body might
399 come from imported lipid rather than *de novo* synthesized fatty acids. And IMD
400 signaling activation is required for this process. Detailed analysis showed that *plin1*
401 downregulation takes charge of LDs' growth in response to transient IMD activation
402 because its expression is suppressed by IMD/Relish activated MRT/PZG complex.
403 These findings indicate that LDs' biogenesis is likely an active host adaptation to

404 immune challenges. As the evidence to further support this hypothesis, we found that
405 enlarged LDs benefits the host against intracellular ROS-mediated oxidative stress,
406 which is tightly associated with IMD activation. Excessive ROS accumulation is often
407 the main cause for inflammation/infection-induced cellular damages. The similar
408 antioxidative function of LDs were also reported in neuron stem cell niche(Bailey et al.,
409 2015) and in cancer cells (Bensaad et al., 2014). However, the detailed mechanism that
410 large LDs prevent ROS accumulation needs further investigation. One possibility is that
411 biological processes such as cancer, neural activity, and inflammation are energy-
412 intensive, rely on robust fat metabolism, which releases amounts of free fatty acid. The
413 oxidation of free fatty acids generates ROS and the growth of LDs efficiently sequester
414 these excessive free lipids. Moreover, large LDs' formation can reduce the opportunity
415 that pathogens make use of free fatty acids for their own proliferation(Arena et al., 2011;
416 LaRock et al., 2015; Narayanan and Edelmann, 2014). That might be why *plin1*
417 deficient flies, owning bigger LDs, had lower bacterial loads after infection. In addition,
418 larger LDs might contain more resident histones, a cationic protein which was reported
419 to be able to kill bacteria in previous study(Anand P et al., 2012). In mammals, IFN-γ
420 treatment of *M. tuberculosis* infected bone-marrow derived macrophage (BMDM) can
421 induce the formation of LDs, in which neutral lipids serve as a source to produce
422 eicosanoids for enhancing the host defense (Knight et al., 2018). Thereby, LDs' growth
423 is beneficial for both redox homeostasis and anti-infection. The downregulation of
424 Plin1 to enlarge LDs might be an effective adaptation for the host to resolve
425 inflammation-associated stress in response to immune activation.

However, during sustained pathogenesis induced either by pathogenic bacterial infection or by hyper-activation of IMD signaling through genetic manipulation, only progressively smaller LDs were observed. We assumed that LDs' growth by autonomous downregulation of endogenous *plin1* in response to IMD activation was unable to overcome robust lipolysis in high energy-consumed hyperinflammation. In consistence, TAGs level in the whole body was continuous decreased either. Interestingly and impressively, although mutation of *plin1* in flies with IMD overactivation enlarged LDs initially, the decomposition of LDs in these flies is instead much faster than flies with IMD hyper-activation alone. Protein translocation assay confirmed that sustained IMD overactivation increased the recruitment of the key rate-limiting lipase, Bmm/ATGL, on the surface of LDs. Furthermore, one finding that *Plin1*$^{-/-}$ mice have a higher rate of ATGL-mediated lipolysis in the adipose tissue (Sohn et al., 2018), supports our notion that Bmm/ATGL-mediated lipolysis might prefer to occur on *plin1* deficient-induced large LDs. As we mentioned above, hyperinflammation leads to the excess accumulation of free fatty acids in the cytoplasm, which will promote lipotoxicity and ROS-induced oxidative stress(Aitken et al., 2006; Koppers et al., 2010; Song et al., 2014). The high level of intracellular ROS can further promote lipolysis and free fatty acids release(Krawczyk SA et al., 2012). This vicious circle finally drives the host enter a severe metaflammation state during chronic hyperinflammation, and subsequently shorten lifespan. A recent study showed that renal purge of hemolymphatic lipids can efficiently prevent ROS-mediated tissue damage in

448 inflammation(Li et al., 2020). In our study, knockdown of Bmm, to prevent free lipids'
449 generation, can also prolonged the lifespan of flies with hyper-inflammation. Therefore,
450 although LDs' growth drove by *plin1* downregulation is an active protection mechanism,
451 high energic wasting in severe pathological condition is more powerful to consume
452 these large LDs very quickly. Instead, *plin1* mutation looks like to enhance the
453 decomposition of large LDs in this case. However, the mechanism of the recruitment
454 of lipases on large LDs in response to hyper-inflammation, and the involvement of Plin1
455 need further investigation.
456
457 Plin1 is an important regulator on the surface of LDs. It has been reported to control
458 the lipid mobilization on LDs surface by recruiting kinds of enzymes(Gandotra et al.,
459 2011; Sztalryd et al., 2003) . We found in this study *plin1* expression is also regulated
460 by innate immune signaling. It promotes us to image that Plin1 may serve as a bridge
461 factor to link immunity and lipid metabolism through modification of LDs. In response
462 to transient immune activation, adaptative enlarged LDs benefit the host against
463 inflammation-related stress; while in prolonged hyper-immune activation, large LDs
464 decompose quickly and enhance lipolysis, which worsen the pathogenesis. The
465 dynamic morphogenesis of LDs in these two conditions are totally different, in both of
466 which Plin1 involved. It is worthy in the future to trace and dissect the dynamic protein
467 composition on the surface of LDs along the different stages of inflammation,
468 especially the ones interacted with Plin1. In sum, we found that the homeostasis of LDs'
469 morphology is critical in the regulation of pathogenesis during infection. And LDs'

470 regulation may provide a potential therapeutic target for resolution of inflammation.

471

472 **Materials and Methods**

473 Detailed information on *Drosophila* stocks and bacterial strain; cloning and double-
474 strand RNAs; infection and survival rate counting; lifespan counting; bacterial loads
475 assay; cell culture, transfection and luciferase assay; qRT-PCR; lipid droplet staining
476 and counting; TAG assay; RU486 treatment; ROS detection; starvation test; microscopy
477 and software; statistical analyses are described in the Supplemental Experimental
478 Procedures.

479

480 **Acknowledgements**

481 We thank Drs. Xun Huang (Institute of Genetics and Developmental Biology, CAS) for
482 providing stocks of *plin1*^{38}, *UAS-plin1* mcherry, *UAS-plin1 RNAi*, *Bmm-GFP* knock-in
483 flies and valuable comments; Yong Liu (Wuhan University) for providing stocks of
484 *UAS-Bmm RNAi* and *UAS-Bmm*. Zhiwei Liu (Shanghai Ocean University) for
485 providing stock of *UAS-gstD-GFP*; Zhihua Liu (Institute of Biophysics, CAS) for
486 providing *S. typhimurium (SR-11)* strain; Ms. Song-qing Liu (Institute of Biophysics,
487 CAS) for fly food preparation and stock maintenance. This work was supported by
488 grants from the Strategic Priority Research Program of the Chinese Academy of
489 Sciences to H.T (XDB29030301) and L.P (XDA13010500), Shanghai S&T Innovation
490 Program (2018SHZDZX05) and MOST BR S&T Program (2018ZX10101004002004)
491 to H.T., the National Natural Science Foundation of China to L.P (31870887) and J.Y

(31670909) and Shanghai Municipal Science and Technology Major Project (2019SHZDZX02). L.P is a fellow of CAS Youth Innovation Promotion Association (2012083).

Author's contributions

Conceptualization, L.W. and L.P.; Methodology and Validation, L.W. and L.P.; Formal Analysis, L.W. J.L., J.Y., Z.F. and L.P.; Investigation, L.W. and L.P.; Resources, L.P.; Writing-Original Draft, L.W. and L.P.; Writing -Review & Editing, L.P.; Supervision, H.T. and L.P.; Funding Acquisition, J.Y., H.T. and L.P.

DECLARATION OF INTERESTS

The authors declare no competing interests.

References

Aitken, R.J., Wingate, J.K., De Iuliis, G.N., Koppers, A.J., and McLaughlin, E.A. (2006). Cis-unsaturated fatty acids stimulate reactive oxygen species generation and lipid peroxidation in human spermatozoa. J Clin Endocrinol Metab *91*, 4154-4163.

Anand P, Cermelli S, L.Z., Kassan A, Bosch M, S.R., Huang L, Ouellette AJ, Pol A, Welte MA, and SP., G. (2012). A novel role for lipid droplets in the organismal antibacterial response. Elife *13*, e00003.

Arena, E.T., Auweter, S.D., Antunes, L.C., Vogl, A.W., Han, J., Guttman, J.A., Croxen, M.A., Menendez, A., Covey, S.D., Borchers, C.H.*, et al.* (2011). The deubiquitinase activity of the Salmonella pathogenicity island 2 effector, SseL, prevents accumulation of cellular lipid droplets. Infect Immun *79*, 4392-4400.

Arita, M. (2012). Mediator lipidomics in acute inflammation and resolution. J Biochem *152*, 313-319.

Arrese, E.L., and Soulages, J.L. (2010). Insect fat body: energy, metabolism, and regulation. Annual review of entomology *55*, 207-225.

Bailey, A.P., Koster, G., Guillermier, C., Hirst, E.M., MacRae, J.I., Lechene, C.P., Postle, A.D., and Gould, A.P. (2015). Antioxidant Role for Lipid Droplets in a Stem Cell Niche of Drosophila. Cell *163*, 340-353.

Bandeira-Melo, C., Phoofolo, M., and Weller, P.F. (2001). Extranuclear lipid bodies, elicited by CCR3-mediated signaling pathways, are the sites of chemokine-enhanced leukotriene C4 production in eosinophils and basophils. The Journal of biological chemistry *276*, 22779-22787.

Barba G, H.F., Harada T, Kohara M, Goulinet S, Matsuura Y, Eder G, Schaff Z, Chapman MJ, Miyamura T, Bréchot C. (1997). Hepatitis C virus core protein shows a cytoplasmic localization and associates to cellular lipid storage droplets. Proc Natl Acad Sci U S A *94*, 1200-1205.

524 Beller M, Riedel D, Jänsch L, Dieterich G, Wehland J, Jäckle H, and RP., K. (2006). Characterization of the
525 Drosophila lipid droplet subproteome. Mol Cell Proteomics *6*, 1082-1094.
526 Beller, M., Bulankina, A.V., Hsiao, H.H., Urlaub, H., Jackle, H., and Kuhnlein, R.P. (2010). PERILIPIN-
527 dependent control of lipid droplet structure and fat storage in Drosophila. Cell Metab *12*, 521-532.
528 Bensaad, K., Favaro, E., Lewis, C.A., Peck, B., Lord, S., Collins, J.M., Pinnick, K.E., Wigfield, S., Buffa, F.M.,
529 Li, J.L*., et al.* (2014). Fatty acid uptake and lipid storage induced by HIF-1alpha contribute to cell growth
530 and survival after hypoxia-reoxygenation. Cell reports *9*, 349-365.
531 Bi, J., Xiang, Y., Chen, H., Liu, Z., Gronke, S., Kuhnlein, R.P., and Huang, X. (2012). Opposite and redundant
532 roles of the two Drosophila perilipins in lipid mobilization. J Cell Sci *125*, 3568-3577.
533 Bickel, P.E., Tansey, J.T., and Welte, M.A. (2009). PAT proteins, an ancient family of lipid droplet proteins
534 that regulate cellular lipid stores. Biochimica et biophysica acta *1791*, 419-440.
535 Blaser, H., Dostert, C., Mak, T.W., and Brenner, D. (2016). TNF and ROS Crosstalk in Inflammation. Trends
536 Cell Biol *26*, 249-261.
537 Brandt, S.M., Dionne, M.S., Khush, R.S., Pham, L.N., Vigdal, T.J., and Schneider, D.S. (2004). Secreted
538 Bacterial Effectors and Host-Produced Eiger/TNF Drive Death in aSalmonella-Infected Fruit Fly. PLoS Biol
539 *2*, e418.
540 Buck, M.D., Sowell, R.T., Kaech, S.M., and Pearce, E.L. (2017). Metabolic Instruction of Immunity. Cell
541 *169*, 570-586.
542 C M Griswold, A L Matthews, K E Bewley, and Mahaffey, J.W. (1993). Molecular Characterization and
543 Rescue of Acatalasemic Mutants of Drosophila Melanogaster. Genetics *134(3)*, 781-788.
544 Cani, P.D., Amar, J., Iglesias, M.A., Poggi, M., Knauf, C., Bastelica, D., Neyrinck, A.M., Fava, F., Tuohy, K.M.,
545 Chabo, C*., et al.* (2007). Metabolic endotoxemia initiates obesity and insulin resistance. Diabetes *56*,
546 1761-1772.
547 Choe, K.M., Werner, T., Stoven, S., Hultmark, D., and Anderson, K.V. (2002). Requirement for a
548 peptidoglycan recognition protein (PGRP) in Relish activation and antibacterial immune responses in
549 Drosophila. Science *296*, 359-362.
550 Clark, R.I., Tan, S.W., Pean, C.B., Roostalu, U., Vivancos, V., Bronda, K., Pilatova, M., Fu, J., Walker, D.W.,
551 Berdeaux, R*., et al.* (2013). MEF2 is an in vivo immune-metabolic switch. Cell *155*, 435-447.
552 Cohen JC, H.J., Hobbs HH. (2011). Human Fatty Liver Disease Old Questions and New Insights. Science
553 *6037*, 1519-1523.
554 D'Avila, H., Melo, R.C.N., Parreira, G.G., Werneck-Barroso, E., Castro-Faria-Neto, H.C., and Bozza, P.T.
555 (2006). Mycobacterium bovis Bacillus Calmette-Guerin Induces TLR2-Mediated Formation of Lipid
556 Bodies: Intracellular Domains for Eicosanoid Synthesis In Vivo. The Journal of Immunology *176*, 3087-
557 3097.
558 den Brok, M.H., Raaijmakers, T.K., Collado-Camps, E., and Adema, G.J. (2018). Lipid Droplets as Immune
559 Modulators in Myeloid Cells. Trends Immunol *39*, 380-392.
560 Dionne, M.S., Pham, L.N., Shirasu-Hiza, M., and Schneider, D.S. (2006). Akt and FOXO dysregulation
561 contribute to infection-induced wasting in Drosophila. Curr Biol *16*, 1977-1985.
562 Ertunc, M.E., and Hotamisligil, G.S. (2016). Lipid signaling and lipotoxicity in metaflammation:
563 indications for metabolic disease pathogenesis and treatment. J Lipid Res *57*, 2099-2114.
564 Fauny, J.D., Silber, J., and Zider, A. (2005). Drosophila Lipid Storage Droplet 2 gene (Lsd-2) is expressed
565 and controls lipid storage in wing imaginal discs. Dev Dyn *232*, 725-732.
566 Feldstein, A.E., Werneburg, N.W., Canbay, A., Guicciardi, M.E., Bronk, S.F., Rydzewski, R., Burgart, L.J.,
567 and Gores, G.J. (2004). Free fatty acids promote hepatic lipotoxicity by stimulating TNF-alpha expression

568 via a lysosomal pathway. Hepatology *40*, 185-194.
569 Fu, S., Yang, L., Li, P., Hofmann, O., Dicker, L., Hide, W., Lin, X., Watkins, S.M., Ivanov, A.R., and
570 Hotamisligil, G.S. (2011). Aberrant lipid metabolism disrupts calcium homeostasis causing liver
571 endoplasmic reticulum stress in obesity. Nature *473*, 528-531.
572 Gandotra S, L.D.C., Bottomley W, Cervera P, Giral P, Reznik Y, Charpentier G, Auclair M, Delépine M,
573 Barroso I, Semple RK, Lathrop M, Lascols O, Capeau J, O'Rahilly S, Magré J, Savage DB, Vigouroux C.
574 (2011). Perilipin Deficiency and Autosomal Dominant Partial Lipodystrophy. N Engl J Med *8*, 740.
575 Gandotra, S., Lim, K., Girousse, A., Saudek, V., O'Rahilly, S., and Savage, D.B. (2011). Human frame shift
576 mutations affecting the carboxyl terminus of perilipin increase lipolysis by failing to sequester the
577 adipose triglyceride lipase (ATGL) coactivator AB-hydrolase-containing 5 (ABHD5). The Journal of
578 biological chemistry *286*, 34998-35006.
579 Greenberg, A.S., Coleman, R.A., Kraemer, F.B., McManaman, J.L., Obin, M.S., Puri, V., Yan, Q.W., Miyoshi,
580 H., and Mashek, D.G. (2011). The role of lipid droplets in metabolic disease in rodents and humans. The
581 Journal of clinical investigation *121*, 2102-2110.
582 Grisouard, J., Bouillet, E., Timper, K., Radimerski, T., Dembinski, K., Frey, D.M., Peterli, R., Zulewski, H.,
583 Keller, U., Muller, B*., et al.* (2012). Both inflammatory and classical lipolytic pathways are involved in
584 lipopolysaccharide-induced lipolysis in human adipocytes. Innate Immun *18*, 25-34.
585 Grönke, S., Beller, M., Fellert, S., Ramakrishnan, H., Jäckle, H., and Kühnlein, R.P. (2003). Control of Fat
586 Storage by a Drosophila PAT Domain Protein. Current Biology *13*, 603-606.
587 Grönke S, M.G., Hirsch J, Fellert S, Andreou A, Haase T, Jäckle H, Kühnlein RP. (2007). Dual lipolytic
588 control of body fat storage and mobilization in Drosophila. PLoS Biol *5(6)*, e137.
589 Gronke, S., Mildner, A., Fellert, S., Tennagels, N., Petry, S., Muller, G., Jackle, H., and Kuhnlein, R.P. (2005).
590 Brummer lipase is an evolutionary conserved fat storage regulator in Drosophila. Cell metabolism *1*,
591 323-330.
592 Guo Y, Walther TC, Rao M, Stuurman N, Goshima G, Terayama K, Wong JS, Vale RD, Walter P, and RV., F.
593 (2008). Functional genomic screen reveals genes involved in lipid-droplet formation and utilization.
594 Nature *7195*, 657-661.
595 Harsh, S., Heryanto, C., and Eleftherianos, I. (2019). Intestinal lipid droplets as novel mediators of host-
596 pathogen interaction in Drosophila. Biol Open *8*.
597 He, X., Yu, J., Wang, M., Cheng, Y., Han, Y., Yang, S., Shi, G., Sun, L., Fang, Y., Gong, S.T*., et al.* (2017).
598 Bap180/Baf180 is required to maintain homeostasis of intestinal innate immune response in Drosophila
599 and mice. Nat Microbiol *2*, 17056.
600 Heier, C., and Kuhnlein, R.P. (2018). Triacylglycerol Metabolism in Drosophila melanogaster. Genetics
601 *210*, 1163-1184.
602 Henne, W.M., Reese, M.L., and Goodman, J.M. (2018). The assembly of lipid droplets and their roles in
603 challenged cells. EMBO J *37*.
604 Herms, A., Bosch, M., Ariotti, N., Reddy, B.J., Fajardo, A., Fernandez-Vidal, A., Alvarez-Guaita, A.,
605 Fernandez-Rojo, M.A., Rentero, C., Tebar, F*., et al.* (2013). Cell-to-cell heterogeneity in lipid droplets
606 suggests a mechanism to reduce lipotoxicity. Curr Biol *23*, 1489-1496.
607 Hoffmann JA. (2003). The immune response of Drosophila. Nature *426*, 33-38.
608 Hope, R.G., Murphy, D.J., and McLauchlan, J. (2002). The domains required to direct core proteins of
609 hepatitis C virus and GB virus-B to lipid droplets share common features with plant oleosin proteins.
610 The Journal of biological chemistry *277*, 4261-4270.
611 Hotamisligil, G. (2017). Foundations of Immunometabolism and Implications for Metabolic Health and

612 Disease. Immunity *3*, 406-420.
613 Itabe, H., Yamaguchi, T., Nimura, S., and Sasabe, N. (2017). Perilipins: a diversity of intracellular lipid
614 droplet proteins. Lipids in health and disease *16*, 83.
615 J P Phillips , S D Campbell, D Michaud, M Charbonneau, and Hilliker, A.J. (1989). Null Mutation of Copper-
616 Zinc Superoxide Dismutase in Drosophila Confers Hypersensitivity to Paraquat and Reduced Longevity.
617 Proc Natl Acad Sci *86(8)*, 2761-2765.
618 JA., H. (2003). The immune response of Drosophila. Nature *426*, 33-38.
619 Kaneko T, G.W., Mellroth P, Steiner H, Fukase K, Kusumoto S, Harley W, Fox A, Golenbock D, Silverman
620 N. (2004). Monomeric and polymeric gram-negative peptidoglycan but not purified LPS stimulate the
621 Drosophila IMD pathway. Immunity *20*, 637-649.
622 Kimmel, A.R., and Sztalryd, C. (2016). The Perilipins: Major Cytosolic Lipid Droplet-Associated Proteins
623 and Their Roles in Cellular Lipid Storage, Mobilization, and Systemic Homeostasis. Annual review of
624 nutrition *36*, 471-509.
625 Kleino, A., and Silverman, N. (2014). The Drosophila IMD pathway in the activation of the humoral
626 immune response. Developmental and comparative immunology *42*, 25-35.
627 Knight, M., Braverman, J., Asfaha, K., Gronert, K., and Stanley, S. (2018). Lipid droplet formation in
628 Mycobacterium tuberculosis infected macrophages requires IFN-gamma/HIF-1alpha signaling and
629 supports host defense. PLoS Pathog *14*, e1006874.
630 Koppers, A.J., Garg, M.L., and Aitken, R.J. (2010). Stimulation of mitochondrial reactive oxygen species
631 production by unesterified, unsaturated fatty acids in defective human spermatozoa. Free Radic Biol
632 Med *48*, 112-119.
633 Krawczyk SA, Haller JF, Ferrante T, Zoeller RA, and BE, C. (2012). Reactive Oxygen Species Facilitate
634 Translocation of Hormone Sensitive Lipase to the Lipid Droplet During Lipolysis in Human Differentiated
635 Adipocytes. PLoS ONE *7*, e34904.
636 Kühnlein (2012). Thematic review series: Lipid droplet synthesis and metabolism: from yeast to man.
637 Lipid droplet-based storage fat metabolism in Drosophila. J Lipid Res *53(8)*, 1430-1436.
638 LaRock, D.L., Chaudhary, A., and Miller, S.I. (2015). Salmonellae interactions with host processes. Nat
639 Rev Microbiol *13*, 191-205.
640 Lemaitre, B., and Hoffmann, J. (2007). The host defense of Drosophila melanogaster. Annual review of
641 immunology *25*, 697-743.
642 Lemaitre, B.a.H., J., (2007). The host defense of Drosophila melanogaster. Annual review of immunology
643 *25*, 697-743.
644 Leulier, F., Parquet, C., Pili-Floury, S., Ryu, J.H., Caroff, M., Lee, W.J., Mengin-Lecreulx, D., and Lemaitre,
645 B. (2003). The Drosophila immune system detects bacteria through specific peptidoglycan recognition.
646 Nature immunology *4*, 478-484.
647 Li, X., Rommelaere, S., Kondo, S., and Lemaitre, B. (2020). Renal Purge of Hemolymphatic Lipids Prevents
648 the Accumulation of ROS-Induced Inflammatory Oxidized Lipids and Protects Drosophila from Tissue
649 Damage. Immunity *52*, 374-387 e376.
650 Listenberger, L.L., Han, X., Lewis, S.E., Cases, S., Farese, R.V., Jr., Ory, D.S., and Schaffer, J.E. (2003).
651 Triglyceride accumulation protects against fatty acid-induced lipotoxicity. Proc Natl Acad Sci U S A *100*,
652 3077-3082.
653 Menon, D., Singh, K., Pinto, S.M., Nandy, A., Jaisinghani, N., Kutum, R., Dash, D., Prasad, T.S.K., and
654 Gandotra, S. (2019). Quantitative Lipid Droplet Proteomics Reveals Mycobacterium tuberculosis
655 Induced Alterations in Macrophage Response to Infection. ACS infectious diseases *5*, 559-569.

656 Morgan, M.J., and Liu, Z.G. (2011). Crosstalk of reactive oxygen species and NF-kappaB signaling. Cell
657 Res *21*, 103-115.
658 Murphy, D. (2001). The biogenesis and functions of lipid bodies in animals, plants and microorganisms.
659 Prog Lipid Res *5*, 325-438.
660 Myllymaki, H., Valanne, S., and Ramet, M. (2014). The Drosophila imd signaling pathway. J Immunol *192*,
661 3455-3462.
662 Narayanan, L.A., and Edelmann, M.J. (2014). Ubiquitination as an efficient molecular strategy employed
663 in salmonella infection. Front Immunol *5*, 558.
664 Neyen, C., Runchel, C., Schüpfer, F., Meier, P., and Lemaitre, B. (2016). The regulatory isoform rPGRP-LC
665 induces immune resolution via endosomal degradation of receptors. Nature immunology *17*, 1150-1158.
666 O'Neill, L.A., Kishton, R.J., and Rathmell, J. (2016). A guide to immunometabolism for immunologists.
667 Nature reviews Immunology *16*, 553-565.
668 Pacheco P, Bozza FA, G.R., Bozza M, W.P., Castro-Faria-Neto HC, and PT., B. (2002). Lipopolysaccharide-
669 induced leukocyte lipid body formation in vivo innate immunity elicited intracellular Loci involved in
670 eicosanoid metabolism.pdf>. J Immunol *1*, 6498-6506.
671 Pereira-Dutra, F.S., Teixeira, L., de Souza Costa, M.F., and Bozza, P.T. (2019). Fat, fight, and beyond: The
672 multiple roles of lipid droplets in infections and inflammation. Journal of leukocyte biology.
673 Peyron, P., Vaubourgeix, J., Poquet, Y., Levillain, F., Botanch, C., Bardou, F., Daffe, M., Emile, J.F., Marchou,
674 B., Cardona, P.J.*, et al.* (2008). Foamy macrophages from tuberculous patients' granulomas constitute a
675 nutrient-rich reservoir for M. tuberculosis persistence. PLoS Pathog *4*, e1000204.
676 Roman, G., Endo, K., Zong, L., and Davis, R.L. (2001). P[Switch], a system for spatial and temporal control
677 of gene expression in Drosophila melanogaster. Proceedings of the National Academy of Sciences of the
678 United States of America *98*, 12602-12607.
679 Saka, H.A., and Valdivia, R. (2012). Emerging roles for lipid droplets in immunity and host-pathogen
680 interactions. Annu Rev Cell Dev Biol *28*, 411-437.
681 Samsa, M.M., Mondotte, J.A., Iglesias, N.G., Assuncao-Miranda, I., Barbosa-Lima, G., Da Poian, A.T.,
682 Bozza, P.T., and Gamarnik, A.V. (2009). Dengue virus capsid protein usurps lipid droplets for viral particle
683 formation. PLoS pathogens *5*, e1000632.
684 Schweiger, M., Romauch, M., Schreiber, R., Grabner, G.F., Hutter, S., Kotzbeck, P., Benedikt, P., Eichmann,
685 T.O., Yamada, S., Knittelfelder, O.*, et al.* (2017). Pharmacological inhibition of adipose triglyceride lipase
686 corrects high-fat diet-induced insulin resistance and hepatosteatosis in mice. Nature communications *8*,
687 14859.
688 Serhan, C.N., Chiang, N., Dalli, J., and Levy, B.D. (2014). Lipid mediators in the resolution of inflammation.
689 Cold Spring Harb Perspect Biol *7*, a016311.
690 Sohn, J.H., Lee, Y.K., Han, J.S., Jeon, Y.G., Kim, J.I., Choe, S.S., Kim, S.J., Yoo, H.J., and Kim, J.B. (2018).
691 Perilipin 1 (Plin1) deficiency promotes inflammatory responses in lean adipose tissue through lipid
692 dysregulation. J Biol Chem.
693 Song, Y., Li, X., Li, Y., Li, N., Shi, X., Ding, H., Zhang, Y., Li, X., Liu, G., and Wang, Z. (2014). Non-esterified
694 fatty acids activate the ROS-p38-p53/Nrf2 signaling pathway to induce bovine hepatocyte apoptosis in
695 vitro. Apoptosis *19*, 984-997.
696 Sorgi, C.A., Secatto, A., Fontanari, C., Turato, W.M., Belanger, C., de Medeiros, A.I., Kashima, S., Marleau,
697 S., Covas, D.T., Bozza, P.T.*, et al.* (2009). Histoplasma capsulatum cell wall {beta}-glucan induces lipid body
698 formation through CD18, TLR2, and dectin-1 receptors: correlation with leukotriene B4 generation and
699 role in HIV-1 infection. J Immunol *182*, 4025-4035.

700 Summers, S.A. (2006). Ceramides in insulin resistance and lipotoxicity. Prog Lipid Res *45*, 42-72.
701 Sykiotis, G.P., and Bohmann, D. (2008). Keap1/Nrf2 signaling regulates oxidative stress tolerance and
702 lifespan in Drosophila. Dev Cell *14*, 76-85.
703 Sztalryd, C., Xu, G., Dorward, H., Tansey, J.T., Contreras, J.A., Kimmel, A.R., and Londos, C. (2003).
704 Perilipin A is essential for the translocation of hormone-sensitive lipase during lipolytic activation. The
705 Journal of cell biology *161*, 1093-1103.
706 Tansey, J.T., Sztalryd, C., Gruia-Gray, J., Roush, D.L., Zee, J.V., Gavrilova, O., Reitman, M.L., Deng, C.X., Li,
707 C., Kimmel, A.R.*, et al.* (2001). Perilipin ablation results in a lean mouse with aberrant adipocyte lipolysis,
708 enhanced leptin production, and resistance to diet-induced obesity. Proc Natl Acad Sci U S A *98*, 6494-
709 6499.
710 Tauchi-Sato, K., Ozeki, S., Houjou, T., Taguchi, R., and Fujimoto, T. (2002). The surface of lipid droplets is
711 a phospholipid monolayer with a unique Fatty Acid composition. The Journal of biological chemistry
712 *277*, 44507-44512.
713 Teixeira, L.s., Rabouille, C., Rørth, P., Ephrussi, A., and Vanzo, N.F. (2003). Drosophila Perilipin/ADRP
714 homologue Lsd2 regulates lipid metabolism. Mechanisms of Development *120*, 1071-1081.
715 Vallochi, A.L., Teixeira, L., Oliveira, K.D.S., Maya-Monteiro, C.M., and Bozza, P.T. (2018). Lipid Droplet, a
716 Key Player in Host-Parasite Interactions. Front Immunol *9*, 1022.
717 Velazquez, A.P., Tatsuta, T., Ghillebert, R., Drescher, I., and Graef, M. (2016). Lipid droplet-mediated ER
718 homeostasis regulates autophagy and cell survival during starvation. The Journal of cell biology *212*,
719 621-631.
720 Vodovar, N., Vinals, M., Liehl, P., Basset, A., Degrouard, J., Spellman, P., Boccard, F., and Lemaitre, B.
721 (2005). Drosophila host defense after oral infection by an entomopathogenic Pseudomonas species.
722 Proceedings of the National Academy of Sciences of the United States of America *102*, 11414-11419.
723 Walpole GFW, G.S., Westman J. (2018). The Role of Lipids in Host–PathogenInteractions. IUBMB Life *5*,
724 384-392.
725 Walther, T.C., and Farese, R.V., Jr. (2012). Lipid droplets and cellular lipid metabolism. Annual review of
726 biochemistry *81*, 687-714.
727 Welte, M.A. (2015). Expanding roles for lipid droplets. Current biology : CB *25*, R470-481.
728 Wiklund, M.L., Steinert, S., Junell, A., Hultmark, D., and Stoven, S. (2009). The N-terminal half of the
729 Drosophila Rel/NF-kappaB factor Relish, REL-68, constitutively activates transcription of specific Relish
730 target genes. Developmental and comparative immunology *33*, 690-696.
731 Yang, S., Zhao, Y., Yu, J., Fan, Z., Gong, S.T., Tang, H., and Pan, L. (2019). Sugar Alcohols of Polyol Pathway
732 Serve as Alarmins to Mediate Local-Systemic Innate Immune Communication in Drosophila. Cell Host
733 Microbe *26*, 240-251 e248.
734 Yao, Y., Li, X., Wang, W., Liu, Z., Chen, J., Ding, M., and Huang, X. (2018). MRT, Functioning with NURF
735 Complex, Regulates Lipid Droplet Size. Cell Rep *24*, 2972-2984.
736 Zu, L., He, J., Jiang, H., Xu, C., Pu, S., and Xu, G. (2009). Bacterial endotoxin stimulates adipose lipolysis
737 via toll-like receptor 4 and extracellular signal-regulated kinase pathway. J Biol Chem *284*, 5915-5926.

738

739 **MAIN FIGURES AND LEGENDS**

740 Including seven main figures.

Figure 1

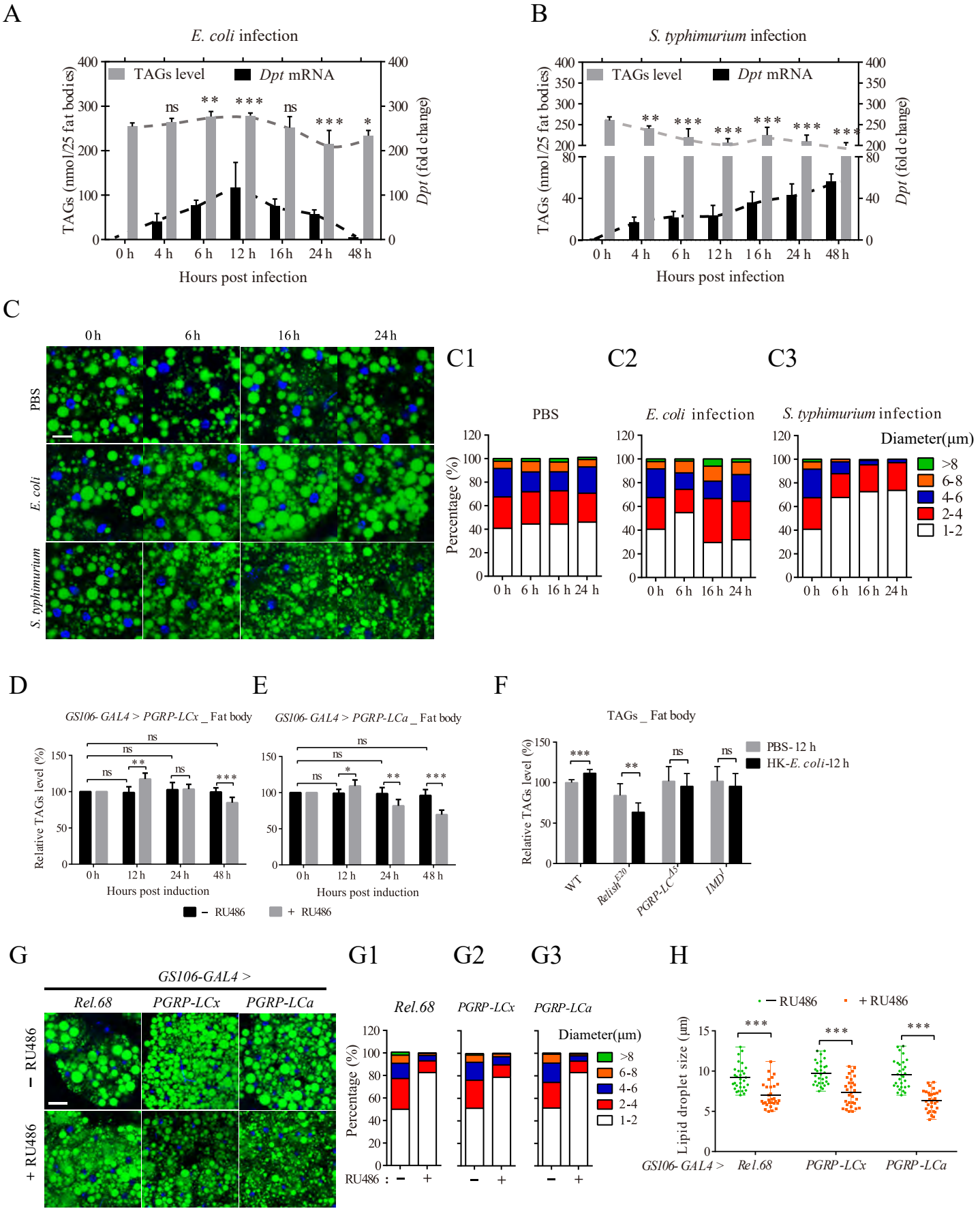
A
E. coli infection
TAGs level
Dpt mRNA
TAGs (nmol/25 fat bodies)
Dpt (fold change)
Hours post infection
0 h
4 h
6 h
12 h
16 h
24 h
48 h
B
S. typhimurium infection
C
PBS
E. coli
S. typhimurium
C1
C2
C3
Percentage (%)
Diameter(μm)
>8
6-8
4-6
2-4
1-2
D
GS106- GAL4 > PGRP-LCx _ Fat body
Relative TAGs level (%)
Hours post induction
– RU486
+ RU486
E
GS106- GAL4 > PGRP-LCa _ Fat body
F
TAGs _ Fat body
PBS- 12 h
HK-E. coli-12 h
WT
Relish E20
PGRP-LC Δ5
IMD 1
G
GS106-GAL4 >
Rel.68
PGRP-LCx
PGRP-LCa
– RU486
+ RU486
G1
G2
G3
RU486 : – +
H
Lipid droplet size (μm)
GS106- GAL4 >

Fig. 1. IMD signaling activation switches lipid metabolism and LDs morphology in the fat body. (**A** and **B**) Relative *Dptericin*(*Dpt*) mRNA expression and TAGs level in the fat body of wild type flies at indicated time points post *E. coli* (**A**) and *S. typhimurium* (**B**) infection. The mean values of *Dpt* mRNA expression or TAGs level were connected by dash line. The fold change of mRNA expression was normalized to that of 0 h and four independent repeats (n =20 flies per repeat) were performed at each time point. Total TAGs level of 25 flies' fat body tissues was quantified in six biological replicates at each time point. (**C**) BODIPY staining (green) of LDs in the fat body of wild type flies at indicated time points post *E. coli* (upper panel) and *S. typhimurium* (lower panel) infection. Nuclei of fat body cells were stained with DAPI (blue). Scale bar: 10 μm. The corresponding statistics of the distribution of LDs' size was shown in (**C1**) for *E. coli* infection and in (**C2**) for *S. typhimurium* infection (n =30 cells for each time point). Eight fat bodies were examined for each time point. (**D** and **E**) Relative changes of TAGs level in the fat body of *GS106-GAL4> PGRP-LCx* (**D**) and *GS106-GAL4> PGRP-LCa* (**E**) flies after RU486 treatment for indicated time. The change of TAG levels was normalized to that of 0h without RU486 treatment. Six independent repeats (n =25 flies per repeat) at each time point were performed. (**F**) Relative TAGs level in the fat body of wild type and IMD pathway mutants (*Relish*，*PGRP-LC* and *Imd*). Each value of TAGs level was normalized to that of 0h of wild type. Each data contains four independent repeats (25 flies' fat body tissues per repeat). (**G**) BODIPY staining (green) of LDs in the fat body of indicated flies after 5 days with (lower panel) or without (upper panel) RU486 treatment (**G**). Nuclei of fat body cells were stained with DAPI (blue). Scale bar: 20 μm. The corresponding statistics of the distribution of LDs' size was shown in (**G1**) for *GS106-GAL4> Rel.68* flies, in (**G2**) for *GS106-GAL4> PGRP-LCx* flies and in (**G3**) for *GS106-GAL4> PGRP-LCa* flies (n =30 cells in each genotype). Eight fat bodies were examined for each sample. (**H**) The statistics of LDs size (n =30 cells) in fat body cells of indicated flies after RU486 treatment for 5 days. Each scattering dot represents the data from one fat body cell. Error bars represent the mean ± s.d. (**A-B, D-F**) and mean with range (**H**). Data were analyzed by One-way ANOVA with Tukey's multiple-comparison test (**A-B, D, E**) and Multiple t-tests (**D-F, H**). $*p < 0.05$; $**p < 0.01$; $***p < 0.001$; ns, not significant. **See also in Supplementary Figure 1.**

Figure 2

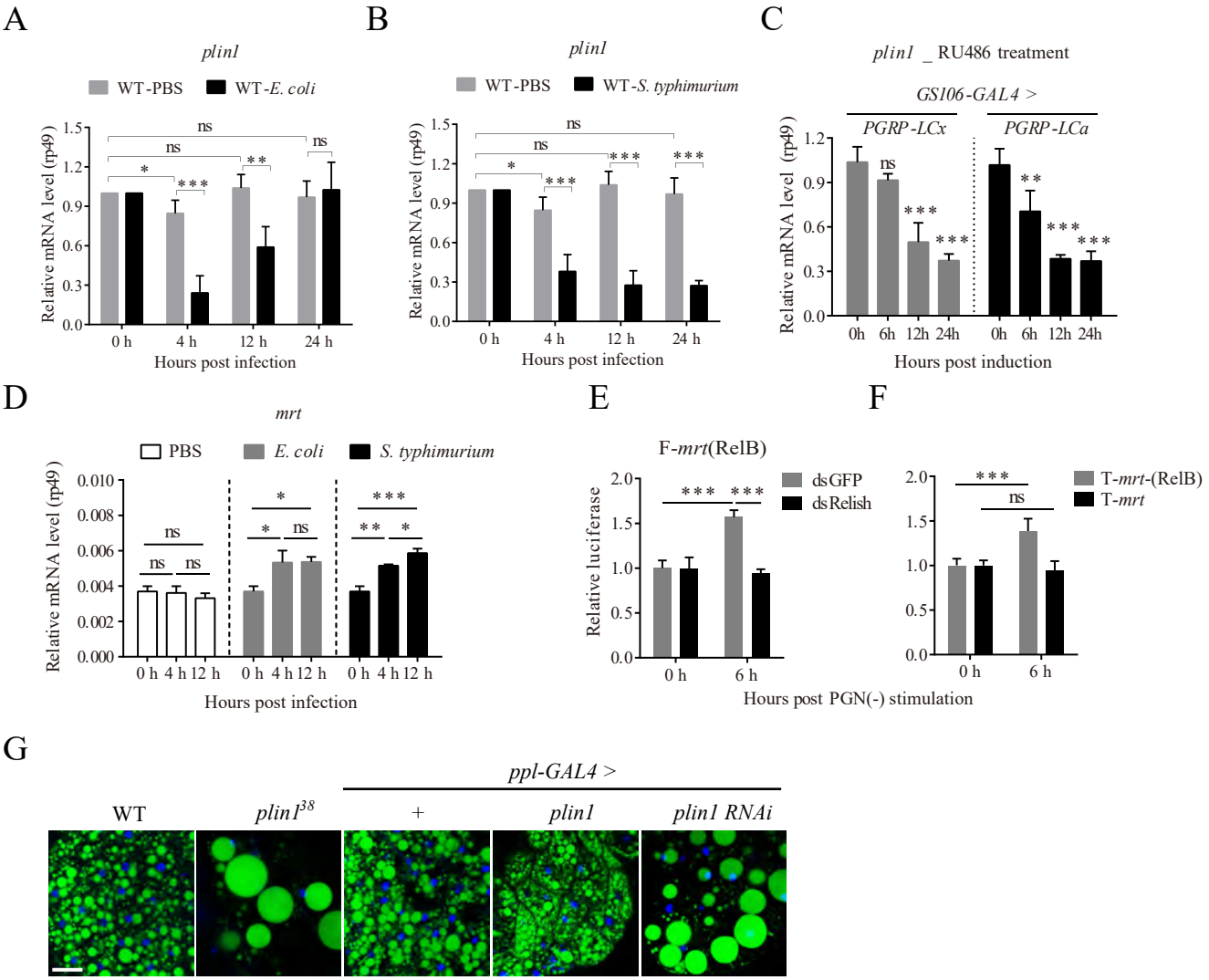
A
plin1
WT-PBS
WT-E. coli
Relative mRNA level (rp49)
Hours post infection
B
plin1
WT-PBS
WT-S. typhimurium
Relative mRNA level (rp49)
Hours post infection
C
plin1 _ RU486 treatment
GS106-GAL4 >
PGRP-LCx
PGRP-LCa
Relative mRNA level (rp49)
Hours post induction
D
mrt
PBS
E. coli
S. typhimurium
Relative mRNA level (rp49)
Hours post infection
E
F-mrt(RelB)
dsGFP
dsRelish
Relative luciferase
F
T-mrt-(RelB)
T-mrt
Hours post PGN(-) stimulation

G
ppl-GAL4 >
WT
plin1^38
+
plin1
plin1 RNAi

Fig. 2. *plin1* responds to IMD activation through Mrt/Pzg complex, and regulates LDs' morphology. (**A and B**) Relative *plin1* mRNA levels in the fat body of wild type flies at the indicated time points post *E. coli* (**A**) or *S. typhimurium* (**B**) infection. Flies treated with sterile PBS were used as a control. The fold change of mRNA expression was normalized to that of 0 h**.** (**C**) Relative *plin1* mRNA levels in the fat body of *GS106-GAL4>PGRP-LCs* flies after RU486 treatment for indicated time. The fold change of mRNA expression was normalized to that of 0 h. (**D**) Relative *mrt* mRNA levels in the fat body of wild type flies post *E. coli* or *S. typhimurium* infection. Flies treated with sterile PBS were used as a control. The fold change of mRNA expression was normalized to that of 0 h. (**E**) Relative luciferase activities of F-*mrt*(RelB) (Full length promoter of -1.5kb to +1bp including all predicted Relish Binding motifs in Fig. S3) reporter in S2* cells after double strand RNA (dsRNA) and PGN (35 μg/ml) treatment. All data were normalized to dsGFP control group at 0 h. Three independent repeats were performed at each time point for each treatment. (**F**) Relative luciferase activities of T-*mrt*(RelB) (Truncated length promoter of -870 to +1bp flanked with two key binding motifs) and T-*mrt* (Truncated length promoter with no binding motifs) reporter in S2* cells after PGN (35 μg/ml) treatment. All data were normalized to T-*mrt*(RelB) group at 0 h. Three independent repeats were performed at each time point for each group. (**G**) BODIPY staining (green) of LDs in the fat body of indicated flies. Nuclei of fat body cells were stained with DAPI (blue). Eight fat bodies were examined for each genotype. Scale bar: 20 μm. Error bars represent the mean ± s.d.. Data were analyzed by One-way ANOVA with Tukey's multiple-comparison test (**A-D**), Multiple t-tests (**A-B**) and Student's t test (**E-F**). $*p < 0.05$; $**p < 0.01$; $***p < 0.001$; ns, no significance. **See also in Supplementary Figure 2 and 3.**

Figure 3

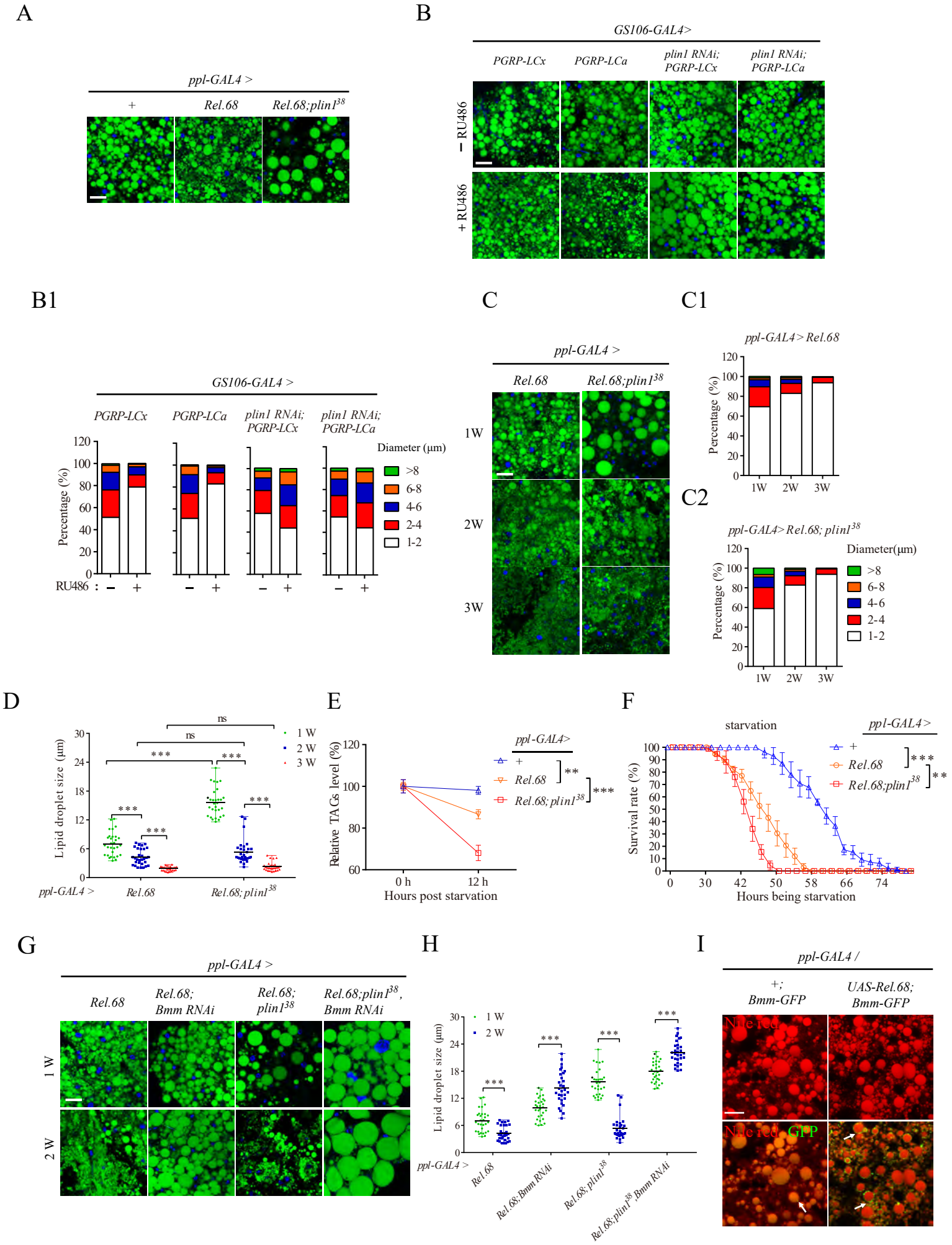
A
ppl-GAL4 >
+
Rel.68
Rel.68;plin1^38
B
GS106-GAL4>
PGRP-LCx
PGRP-LCa
plin1 RNAi; PGRP-LCx
plin1 RNAi; PGRP-LCa
− RU486
+ RU486
B1
GS106-GAL4 >
Percentage (%)
Diameter (μm)
>8
6-8
4-6
2-4
1-2
RU486 : − +
C
ppl-GAL4 >
Rel.68
Rel.68;plin1^38
1W
2W
3W
C1
ppl-GAL4> Rel.68
C2
ppl-GAL4> Rel.68; plin1^38
D
Lipid droplet size (μm)
1 W
2 W
3 W
ns
***
ppl-GAL4 >
Rel.68
Rel.68; plin1^38
E
Relative TAGs level (%)
ppl-GAL4>
+
Rel.68
Rel.68; plin1^38
**
***
0 h
12 h
Hours post starvation
F
starvation
ppl-GAL4>
Survival rate (%)
Hours being starvation
G
ppl-GAL4 >
Rel.68
Rel.68; Bmm RNAi
Rel.68; plin1^38
Rel.68;plin1^38, Bmm RNAi
1 W
2 W
H
Lipid droplet size (μm)
ppl-GAL4 >
Rel.68
Rel.68;Bmm RNAi
Rel.68; plin1^38
Rel.68;plin1^38 Bmm RNAi
I
ppl-GAL4 /
+; Bmm-GFP
UAS-Rel.68; Bmm-GFP
Nile red
Nile red GFP

Fig. 3. *S*ustained IMD activation prefers to enhance Bmm-mediated lipolysis on large LDs. (**A**) BODIPY staining (green) of LDs in the fat body of indicated flies. Nuclei of fat body cells were stained with DAPI (blue). Eight fat bodies were examined for each genotype. Scale bar: 20 μm. (**B**) BODIPY staining (green) of LDs (**B**) and statistics of the size distribution of LDs (**B1**) in the fat body of indicated flies after RU486 treatment for 5 days. Nuclei of fat body cells were stained with DAPI (blue). Eight fat bodies were examined for each sample. Scale bar: 20 μm. (**C** and **D**) BODIPY staining (green) of LDs in the fat body of *ppl-GAL4>Rel.68* and *ppl-GAL4>Rel.68,plin*^{38} adult flies (up panel, one-week age; middle panel, two-week age; low panel, three-week age). The corresponding statistics of the distribution of LDs' size was shown in (**C1**) for *ppl-GAL4>Rel.68* flies and in (**C2**) for *ppl-GAL4>Rel.68,plin*^{38} flies (n =30 cells), and the corresponding statistics of the average size of LDs (**D**). Nuclei of fat body cells were stained with DAPI (blue). Eight fat bodies were examined for each sample. Scale bars: 20 μm. (**E**) Relative TAGs level in the whole body of indicated flies before/after starvation. The change of TAG levels was normalized to that of 0 h for each genotype. Six independent replicates for each sample were performed (n =12 per repeat). (**F**) Survival curves of indicated flies (n = 60) with starvation. (**G** and **H**) BODIPY staining (green) of LDs (**G**) and the corresponding statistics of the average size of LDs (n =30 cells) (**H**) in the fat body of indicated adult flies (up panel, one-week age; low panel, two-week age). Eight fat bodies were examined for each sample. Each scattering dot represents the data from one fat body cell. Nuclei of fat body cells were stained with DAPI (blue). Scale bars: 20 μm. (**I**) Nile red staining (red) of LDs and Bmm-GFP located on the surface of LDs (green) in the fat body of indicated flies. Arrow indicated contact site of LDs. Eight fat bodies were examined for each genotype. Scale bars: 10 μm. Values of plotted curves represent mean ± s.d. of at least three independent repeats (**E-F**). Error bars represent the mean with range (**D, H**). Data were analyzed by Student t-tests (**D-E**), Multiple t-tests (**H**) and Kaplan–Meier (**F**). $^{**}p < 0.01$; $^{***}p < 0.001$; ns, no significance. **See also in Supplementary Figure 4.**

Figure 4

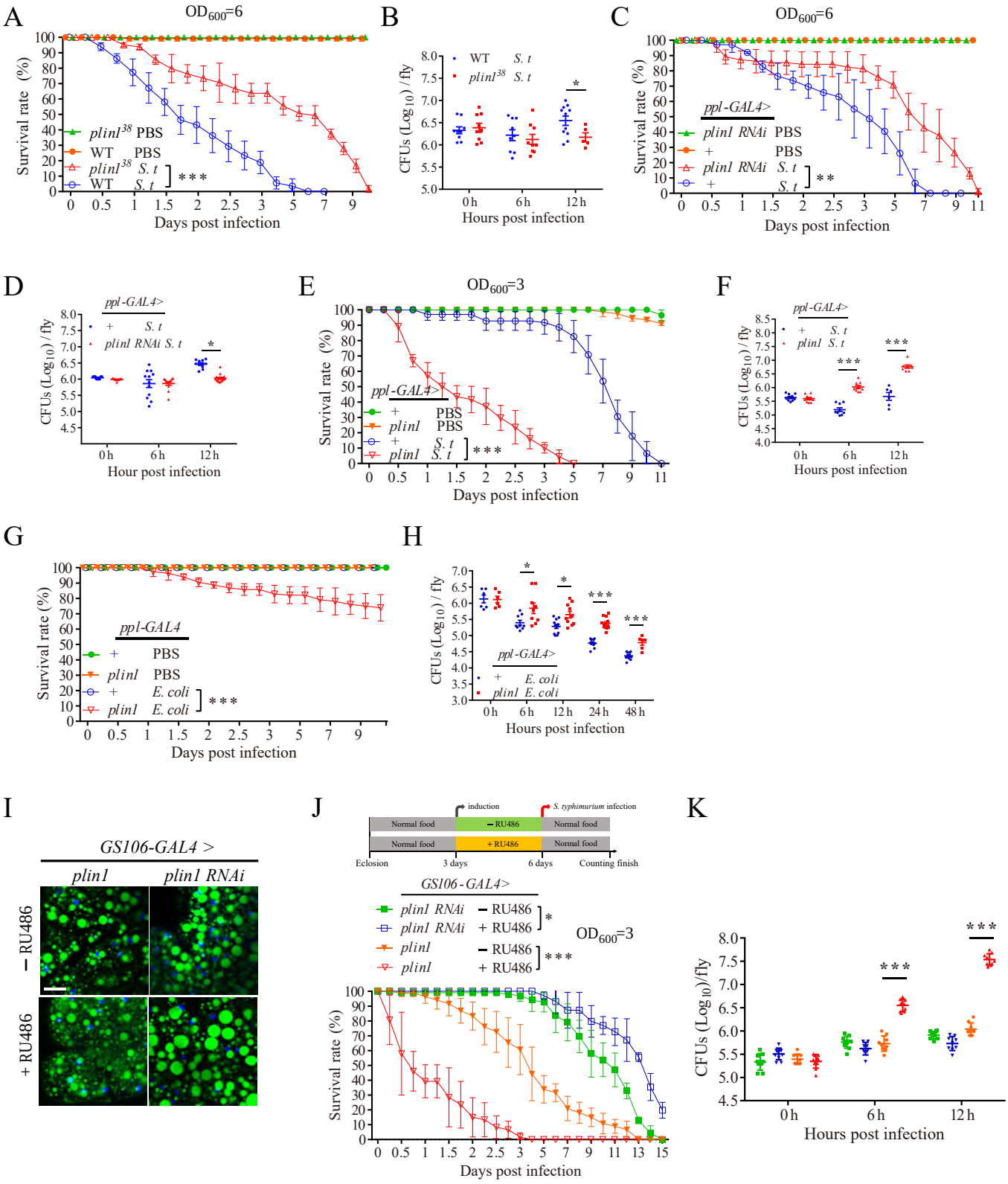
A
OD600=6
Survival rate (%)
plin1 38 PBS
WT PBS
plin1 38 S. t
WT S. t
***
Days post infection
B
CFUs (Log10) / fly
WT S. t
plin1 38 S. t
*
0 h
6 h
12 h
Hours post infection
C
OD600=6
Survival rate (%)
ppl-GAL4>
plin1 RNAi PBS
+ PBS
plin1 RNAi S. t
+ S. t
**
Days post infection
D
ppl-GAL4>
+ S. t
plin1 RNAi S. t
*
Hour post infection
E
OD600=3
Survival rate (%)
ppl-GAL4>
+ PBS
plin1 PBS
+ S. t
plin1 S. t
***
Days post infection
F
ppl-GAL4>
+ S. t
plin1 S. t
***
Hours post infection
G
Survival rate (%)
ppl-GAL4
+ PBS
plin1 PBS
+ E. coli
plin1 E. coli
***
Days post infection
H
CFUs (Log10) / fly
ppl-GAL4>
+ E. coli
plin1 E. coli
24 h
48 h
Hours post infection
I
GS106-GAL4 >
plin1
plin1 RNAi
− RU486
+ RU486
J
induction
S. typhimurium infection
Normal food
− RU486
+ RU486
Eclosion
3 days
6 days
Counting finish
GS106-GAL4>
plin1 RNAi − RU486
plin1 RNAi + RU486
plin1 − RU486
plin1 + RU486
OD600=3
Survival rate (%)
Days post infection
K
CFUs (Log10)/fly
Hours post infection

Fig. 4. *plin1* participates in the susceptibility of flies to bacterial infection. (**A** and **B**) Survival curves (**A**) and bacterial loads (CFUs) (**B**) of wild type and *plin1*^{38} flies (n =60) post *S. typhimurium* infection. (**C** and **D**) Survival curves (**C**) and bacterial loads (CFUs) (**D**) of *ppl-GAL4>plin1 RNAi* and control flies (n =60) post *S. typhimurium* infection. (**E** and **F**) Survival curves (**E**) and bacterial loads (CFUs) (**F**) of *ppl-GAL4>plin1* and control flies (n =60) post *S. typhimurium* infection. (**G** and **H**) Survival curves (**G**) and bacterial loads (CFUs) (**H**) of *ppl-GAL4>plin1* and control flies (n =60) post *E. coli* infection. (**I**) BODIPY staining (green) of LDs in the fat body of *GS106-GAL4>plin1* and *GS106-GAL4>plin1 RNAi* flies after 3 days with (lower panel) or without (upper panel) RU486 treatment. Eight fat bodies were examined for each sample. Scale bar: 20 μm. (**J** and **K**) Survival curves (**J**) and bacterial loads (CFUs) (**K**) of above flies (*I*) (n =60) post *S. typhimurium* infection. Values of plotted curves represent mean ± s.d. (**A, C, E, G, J**) of at least three independent repeats. Each scattering dot (CFUs) represents one technical replicate, line represents the mean of four independent repeats (**B, D, F, H, K**). Data were analyzed by Kaplan–Meier (**A, C, E, G, J**) and Multiple t-tests (**B, D, F, H, K**). *$p < 0.05$; ** $p < 0.01$; *** $p < 0.001$. **See also in Supplementary Figure 5.**

Figure 5

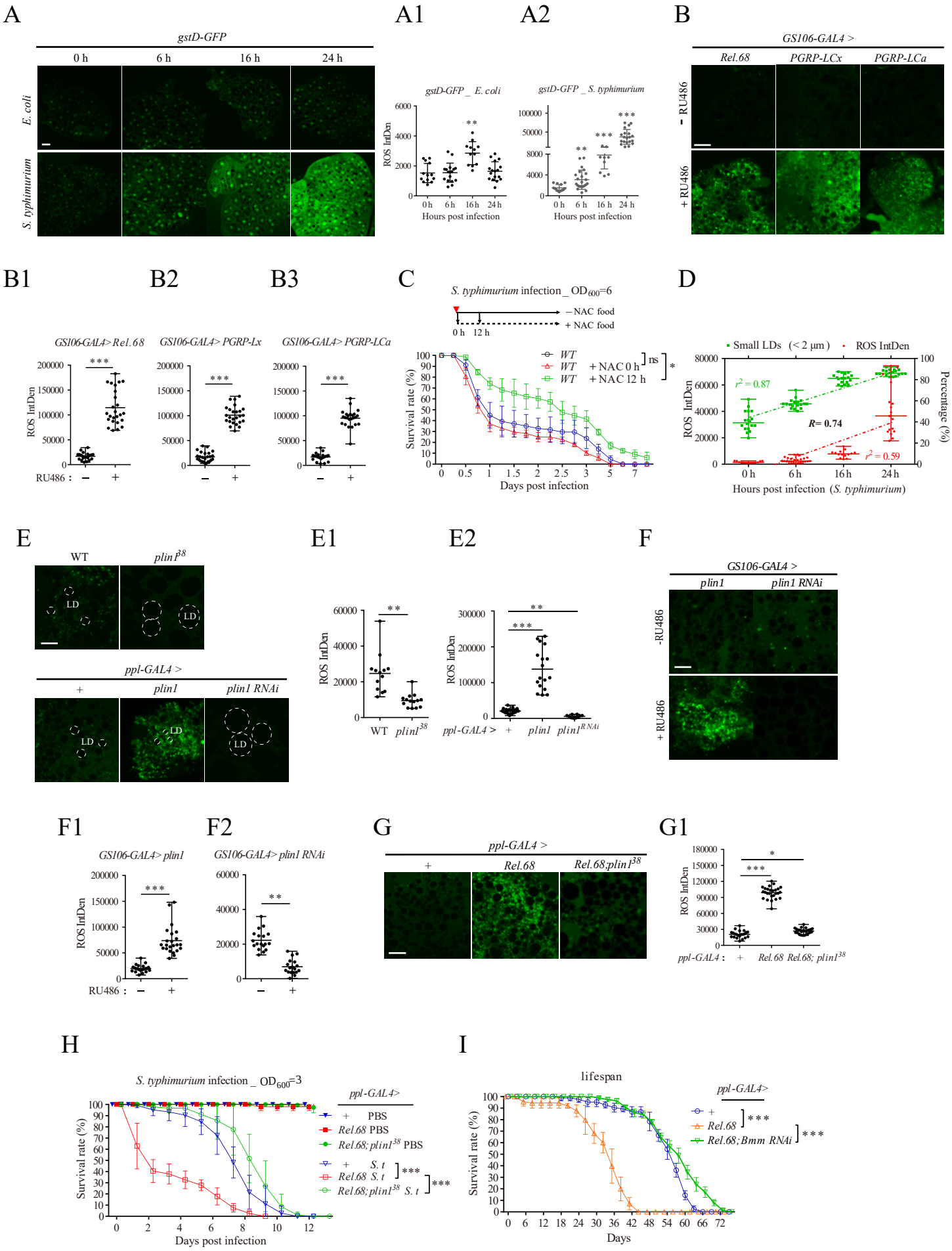
A
gstD-GFP
0 h
6 h
16 h
24 h
E. coli
S. typhimurium
A1
gstD-GFP _ E. coli
ROS IntDen
Hours post infection
A2
gstD-GFP _ S. typhimurium
B
GS106-GAL4 >
Rel.68
PGRP-LCx
PGRP-LCa
- RU486
+ RU486
B1
GS106-GAL4> Rel.68
B2
GS106-GAL4> PGRP-Lx
B3
GS106-GAL4> PGRP-LCa
RU486 :
C
S. typhimurium infection _ OD600=6
– NAC food
+ NAC food
0 h
12 h
WT
WT + NAC 0 h
WT + NAC 12 h
ns
Survival rate (%)
Days post infection
D
Small LDs (< 2 μm)
ROS IntDen
Percentage (%)
R= 0.74
Hours post infection (S. typhimurium)
E
WT
plin1 38
LD
ppl-GAL4 >
+
plin1
plin1 RNAi
E1
E2
F
GS106-GAL4 >
plin1
plin1 RNAi
-RU486
+ RU486
F1
GS106-GAL4> plin1
F2
GS106-GAL4> plin1 RNAi
G
ppl-GAL4 >
Rel.68
Rel.68;plin1 38
G1
ppl-GAL4 :
Rel.68 Rel.68; plin1 38
H
S. typhimurium infection _ OD600=3
ppl-GAL4>
PBS
Rel.68 PBS
Rel.68; plin1 38 PBS
S. t
Rel.68 S. t
Rel.68; plin1 38 S. t
Survival rate (%)
Days post infection
I
lifespan
Rel.68
Rel.68;Bmm RNAi
Days

Fig. 5. The formation of large LDs ameliorates sustained inflammation induced oxidative stress. (**A**) ROS level indicated by GFP intensity (green) of *gstD-GFP* reporter in the fat body of wild type flies infected with *E. coli* (upper panel) or *S. typhimurium* (lower panel) at indicated time points. The statistics of GFP intensity was plotted in (**A1**) for *E. coli* infection and in (**A2**) for *S. typhimurium* infection. Eight fat bodies were examined for each sample and each scattering dot represents the data from one image. Scale bar: 20 μm. (**B**) ROS level indicated by DCFH-DA staining (green) in the fat body of indicated flies with (lower panel) or without (Upper panel) RU486 treatment for 5 days. The statistics of fluorescence intensity was plotted in (**B1**) for *GS106-GAL4>Rel.68* flies, in (**B2**) for *GS106-GAL4>PGRP-LCx* flies and in (**B3**) for *GS106-GAL4>PGRP-LCa* flies. Eight fat bodies were examined for each sample and each scattering dot represents the data from one image. Scale bar: 20 μm. (**C**) Survival curves of wild type flies (n=60 flies) with or without NAC treatment at indicated time post *S. typhimurium* infection. (**D**) Correlation analysis between the percentage of small LDs (< 2 μm, green) and intracellular ROS level (red) in fat body cells at indicated time points post *S. typhimurium* infection. The regression analysis was performed, respectively. Red regression dash line presents the change of intracellular ROS level (r^2 = 0.59) and green regression dash line present the change of small LDs percentage (r^2 = 0.87). The Pearson's correlation of these two set of data was analyzed (Pearson's correlation coefficient R=0.74). (**E**) ROS level indicated by DCFH-DA staining (green) in the fat body of indicated flies. The statistics of fluorescence intensity was plotted in (**E1**) for *plin1*^{38} and in (**E2**) for *ppl-GAL4>plin1* and *ppl-GAL4>plin1-RNAi* flies and their genetic controls, respectively. Dashed circle indicated LDs. Eight fat bodies were examined for each sample and each scattering dot represents the data from one image. Scale bar: 20 μm. (**F**) ROS level indicated by DCFH-DA staining (green) in the fat body of indicated flies with (lower panel) or without (upper panel) RU486 treatment for 5 days. The statistics of fluorescence intensity was plotted in (**F1**) for *GS106-GAL4>plin1* and in (**F2**) for *GS106-GAL4>plin1 RNAi* flies. Eight fat bodies were examined for each sample and each scattering dot represents the data from one image. Scale bar: 20 μm. (**G**) ROS level indicated by DCFH-DA staining (green) in the fat body of *ppl-GAL4>Rel.68*，*ppl-GAL4>Rel.68, plin*^{38} flies and control flies. The corresponding fluorescence intensity was quantified in (**G1**). Eight fat bodies were examined for each sample and each scattering dot represents the data from one image. Scale bar: 20 μm. (**H**) Survival curves of *ppl-GAL4>Rel.68*, *ppl-GAL4>Rel.68,plin*^{38} one-week old adult flies and control flies (n =60) after *S. typhimurium* infection. PBS injection as a control. (**I**) The lifespan curves of indicated flies at normal condition (n =60 per genotype). Error bars represent the mean with range (**A1-2, B1-3, C, E1-2, F1-2, G1**). Values of plotted curves represent mean ± s.d. of at least three independent repeats (**C, H, I**). Data was analyzed by One-Way ANOVA with Tukey's multiple-comparison test (**A1-2, E2, G1**), Student's t test (**B1-3, E1-2, F1-2**) and Kaplan–Meier (**C, H, I**). $^{*}p < 0.05$; $^{**}p < 0.01$; $^{***}p < 0.001$.

Figure 6

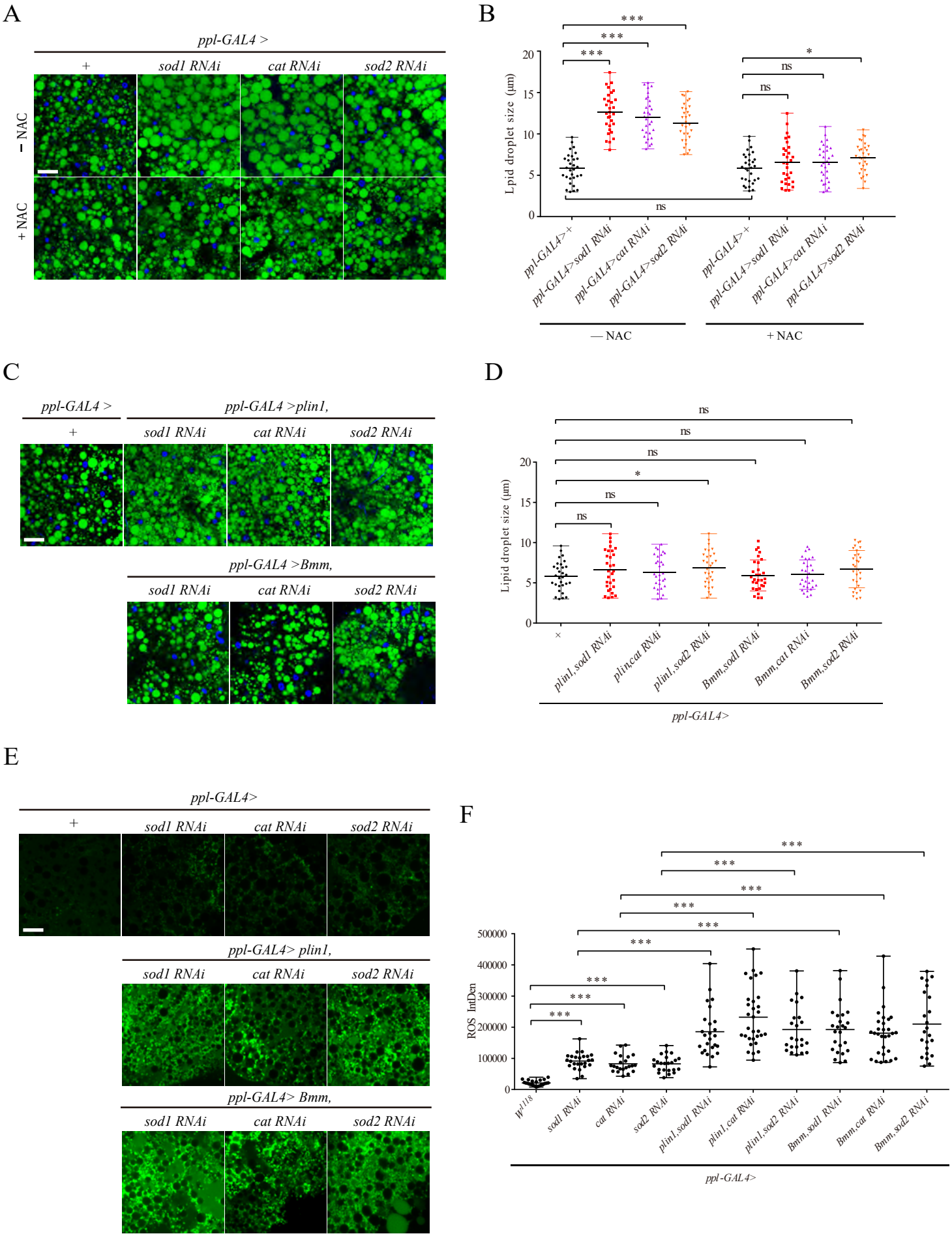
A
ppl-GAL4 >
+
sod1 RNAi
cat RNAi
sod2 RNAi
− NAC
+ NAC
B
Lpid droplet size (μm)
ppl-GAL4>+
ppl-GAL4>sod1 RNAi
ppl-GAL4>cat RNAi
ppl-GAL4>sod2 RNAi
— NAC
+ NAC
C
ppl-GAL4 >
ppl-GAL4 >plin1,
ppl-GAL4 >Bmm,
D
Lipid droplet size (μm)
plin1,sod1 RNAi
plincat RNAi
plin1,sod2 RNAi
Bmm,sod1 RNAi
Bmm,cat RNAi
Bmm,sod2 RNAi
ppl-GAL4>
E
ppl-GAL4> plin1,
ppl-GAL4> Bmm,
F
ROS IntDen
w1118
sod1 RNAi
cat RNAi
sod2 RNAi
plin1,sod1 RNAi
plin1,cat RNAi
plin1,sod2 RNAi
Bmm,sod1 RNAi
Bmm,cat RNAi
Bmm,sod2 RNAi
ppl-GAL4>

Fig. 6. Adaptive large LDs formation contributes to eliminate excessive intracellular ROS. (**A** and **B**) BODIPY staining (green) of LDs (**A**) and the corresponding statistics of LDs' size (n =30 cells) (**B**) in the fat body of indicated flies after 5 days with (lower panel) or without (upper panel) N-acetyl-L-cysteine (NAC) treatment. Eight fat bodies were examined for each sample. Scale bar: 20 μm. (**C** and **D**) BODIPY staining (green) of LDs (**C**) and the corresponding statistics of LDs' size (n =30 cells) (**D**) in the fat body of indicated one-week old adult flies. Eight fat bodies were examined for each sample. Scale bar: 20 μm. (**E** and **F**) ROS levels indicated by DCFH-DA staining (green) in the fat body of indicated one-week old adult flies and control flies (**E**). The corresponding fluorescence intensity was quantified in (**F**). Eight fat bodies were examined for each sample and each scattering dot represents the data from one image. Scale bar: 20 μm. Error bars represent the mean with range. Data was analyzed by One-Way ANOVA with Tukey's multiple-comparison test (**B, D, F**) and Student's t test (**B, F**). *$p < 0.05$; ***$p < 0.001$; ns, no significance.

Figure 7

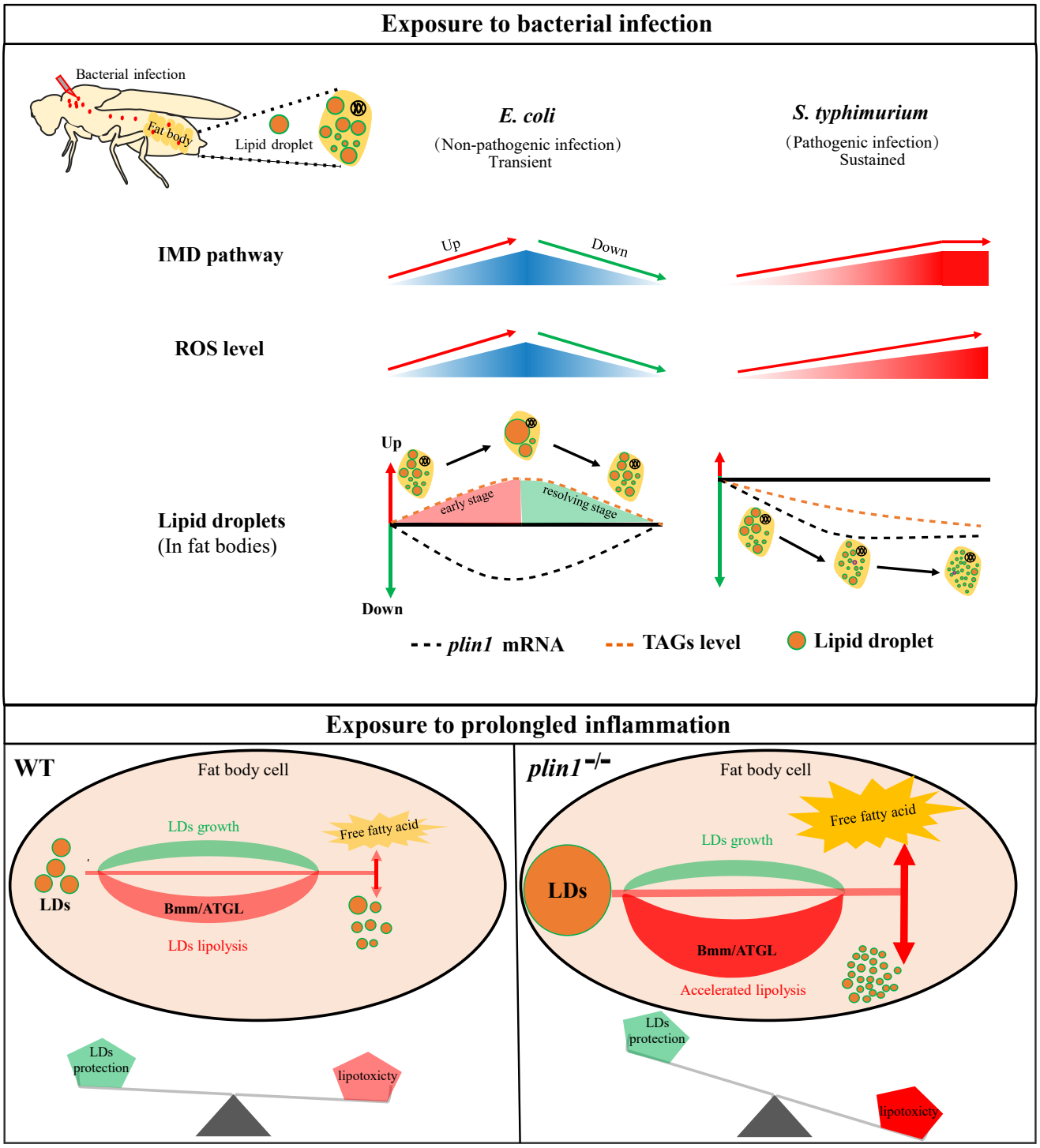
Exposure to bacterial infection
Bacterial infection
Fat body
Lipid droplet
E. coli
(Non-pathogenic infection)
Transient
S. typhimurium
(Pathogenic infection)
Sustained
IMD pathway
Up
Down
ROS level
Lipid droplets
(In fat bodies)
Up
Down
early stage
resolving stage
plin1 mRNA
TAGs level
Lipid droplet
Exposure to prolongled inflammation
WT
Fat body cell
LDs growth
Free fatty acid
LDs
Bmm/ATGL
LDs lipolysis
LDs protection
lipotoxicity
plin1 -/-
Fat body cell
Free fatty acid
LDs growth
LDs
Bmm/ATGL
Accelerated lipolysis
LDs protection
lipotoxicity

Fig. 7. The schematic diagram of LDs' morphogenesis mediated by Plin1 during infection-induced pathogenesis. LD's growth induced by downregulation of *plin1* at early-stage of *E. coli* infection. And enlarged LDs provides antioxidant role and benefits the host for anti-infection. While, sustained hyper-inflammation induced either by *S. typhimurium* infection or genetic manipulation triggers progressively enhanced LDs' lipolysis. And *plin1* deficiency accelerates excessive decomposition of large LDs, which results in energy wasting and severe lipotoxicity, thus deteriorated pathogenesis.

SUPPLEMENTAL INFORMATION

Supplemental Information includes five figures, and one table.

Supplementary Figure Legends

Figure S1

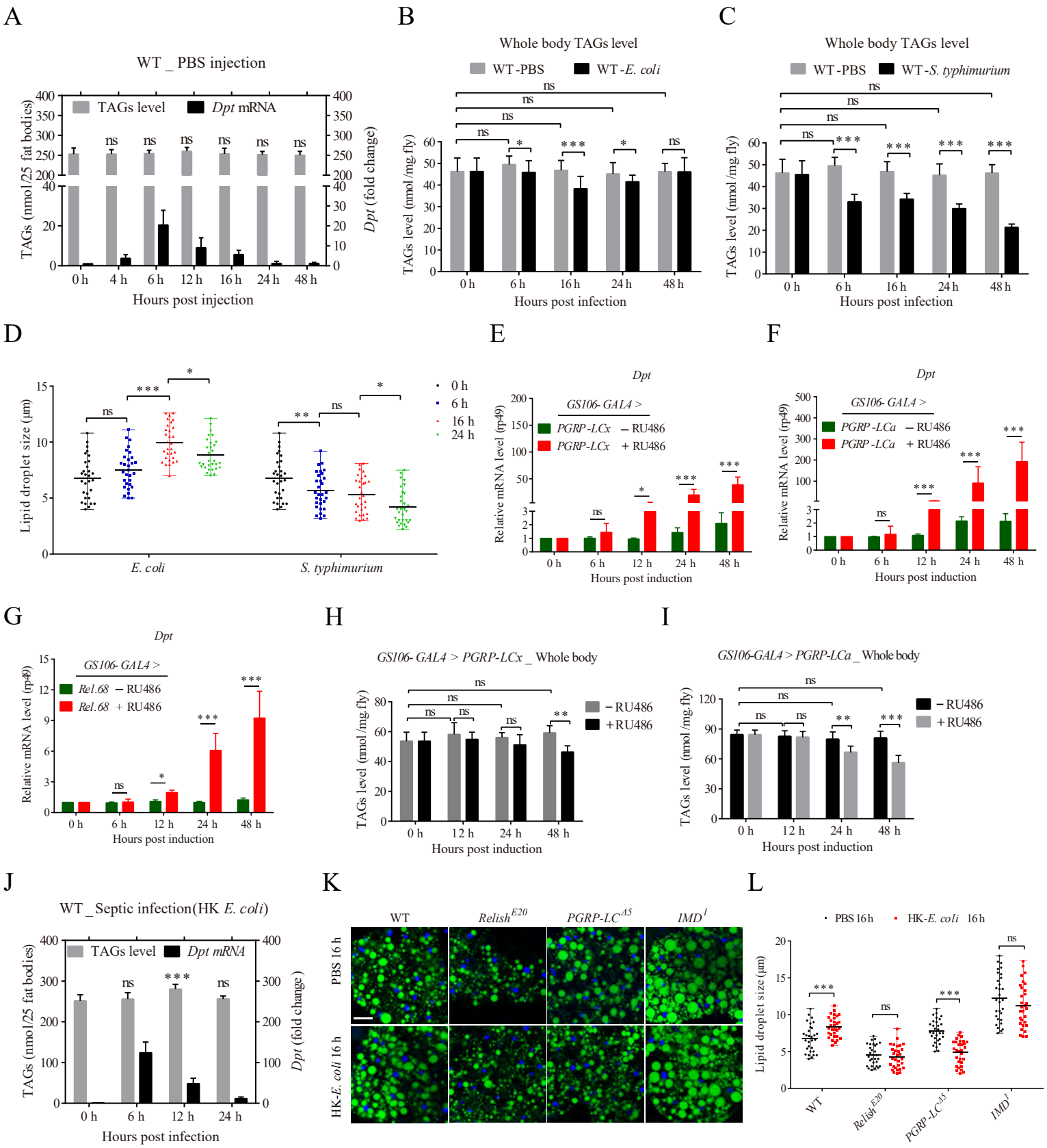
A
WT _ PBS injection
TAGs level
Dpt mRNA
TAGs (nmol/25 fat bodies)
Dpt (fold change)
0 h
4 h
6 h
12 h
16 h
24 h
48 h
Hours post injection
B
Whole body TAGs level
WT-PBS
WT-E. coli
TAGs level (nmol/mg fly)
Hours post infection
C
Whole body TAGs level
WT-PBS
WT-S. typhimurium
TAGs level (nmol/mg fly)
Hours post infection
D
Lipid droplet size (μm)
0 h
6 h
16 h
24 h
E. coli
S. typhimurium
E
Dpt
GS106-GAL4 >
PGRP-LCx – RU486
PGRP-LCx + RU486
Relative mRNA level (rp49)
Hours post induction
F
Dpt
GS106-GAL4 >
PGRP-LCa – RU486
PGRP-LCa + RU486
Relative mRNA level (rp49)
Hours post induction
G
Dpt
GS106-GAL4 >
Rel.68 – RU486
Rel.68 + RU486
Relative mRNA level (rp49)
Hours post induction
H
GS106-GAL4 > PGRP-LCx _ Whole body
– RU486
+RU486
TAGs level (nmol/mg fly)
Hours post induction
I
GS106-GAL4 > PGRP-LCa _ Whole body
– RU486
+RU486
TAGs level (nmol/mg fly)
Hours post induction
J
WT _ Septic infection(HK E. coli)
TAGs level
Dpt mRNA
TAGs (nmol/25 fat bodies)
Dpt (fold change)
Hours post infection
K
WT
Relish^E20
PGRP-LC^Δ5
IMD^1
PBS 16 h
HK-E. coli 16 h
L
PBS 16 h
HK-E. coli 16 h
Lipid droplet size (μm)
WT
Relish^E20
PGRP-LC^Δ5
IMD^1

Fig. S1. IMD signaling modifies lipid metabolism and LDs morphology. Related to Figure 1. (**A**) Relative *Dptericin* (*Dpt*) mRNA expression (black) and TAGs level (gray) in the fat body of wild type flies at indicated time points after sterile PBS injection. The fold change of mRNA expression was normalized to that of 0 h and four independent repeats (n =20 flies per repeat) were performed at each time point. Total TAGs level of 25 flies' fat body tissues was quantified in six biological replicates at each time point. (**B** and **C**) Relative TAGs levels in the whole body of wild type flies at indicated time points post *E. coli* (**B**) or *S. typhimurium* (**C**) infection. Sterile PBS injection as a control. The change of TAG levels was normalized to that of 0 h, respectively. Six independent replicates for each time point were performed (n =12 flies per replicate). (**D**) The statistics of LDs' size (n =30 cells) in the fat body of wild type flies at indicated time point post *E. coli* or *S. typhimurium* infection. Each scattering dot represents the data from one fat body cell. (**E-G**) Relative *Dpt* mRNA expression in the fat body of *GS106-GAL4> PGRP-LCx* (**E**) and *GS106-GAL4> PGRP-LCa* (**F**) and *GS106-GAL4>Rel.68* (**G**) flies at indicated time point after with or without RU486 feeding. The data was normalized to that of 0 h without RU486 treatment. Four independent repeats at each time point were performed (n = 20 per repeat). (**H** and **I**) TAGs level in the whole body of *GS106-GAL4> PGRP-LCx* (**H**) and *GS106-GAL4> PGRP-LCa* (**I**) flies at indicated time point after with or without RU486 feeding. Six independent replicates for each time point were performed (n =12 flies in each replicate). (**J**) Relative *Dptericin* (*Dpt*) mRNA expression (black) and TAGs level (Grey) in the fat body of wild type flies at indicated time points post heat-killed *E. coli* (HK-*E. coli*) infection. The sample were treated and analyzed in the same way as above (**A**) described. (**K-L**) BODIPY staining (green) of LDs (**K**) and the corresponding statistics of LDs' size (n =30 cells) (**L**) in the fat body of IMD pathway mutant flies and corresponding genetic control flies. Eight fat bodies were examined for each sample. Scale bar: 20 μm. Error bars represent mean ± s.d. (**A-C, E-J**) or mean with range (**D, L**). Data were analyzed by One-way ANOVA with Tukey's multiple-comparison test (**A-D, H-J**) and Multiple t-tests (**B-C, E-I, L**). *$p < 0.05$; ** $p < 0.01$;*** $p < 0.001$; ns, no significance.

Figure S2

A

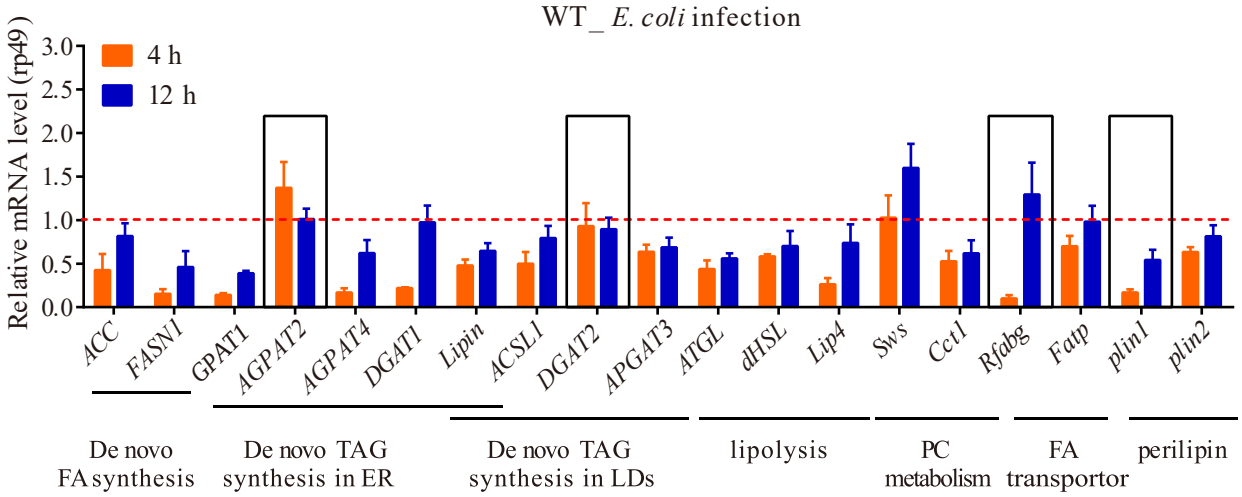

B

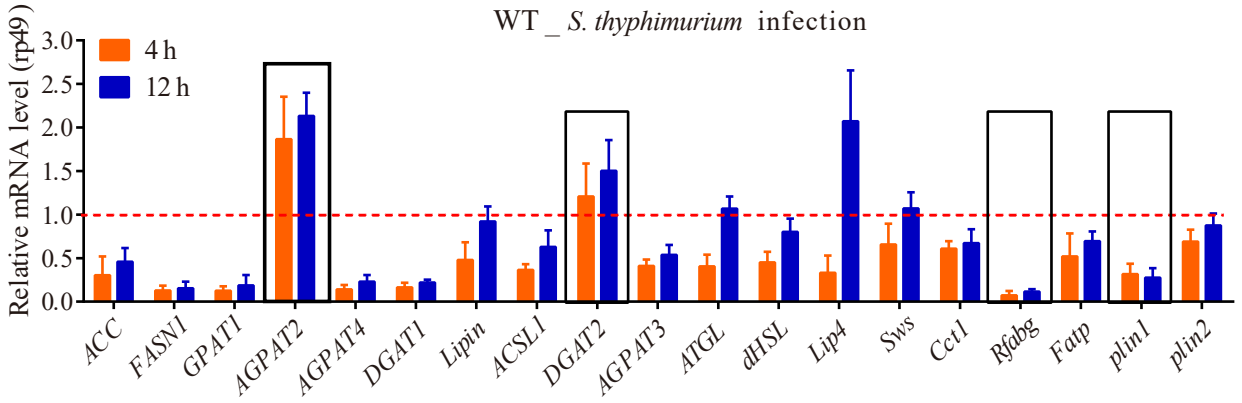

C

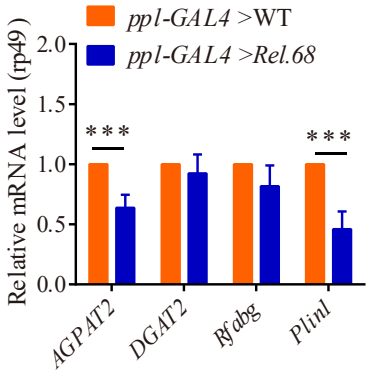

Fig. S2. The expression profile of genes involved in the regulation of LDs metabolism during IMD activation. Related to Figure 2. (**A** and **B**) Relative mRNA expression of a set of genes related to LD metabolism in the fat body of wild type flies at the indicated time points post *E. coli* (**A**) or *S. typhimurium* (**B**) infection. All measurements were normalized to that of 0 h (red line). Four independent repeats at each time point were performed (n = 20 per repeat). (**C**) Relative mRNA expression of genes *APGAT2*, *DGAT2*, *Rfabg* and *Plin1* in the fat body of *ppl-GAL4>Rel.68* flies compared with its genetic control flies of *ppl-GAL4> +*. Four independent repeats at each time point were performed (n = 20 per repeat). Error bars represent mean ± s.d.. Data were analyzed by Multiple t-tests. *** $p < 0.001$.

Figure S3

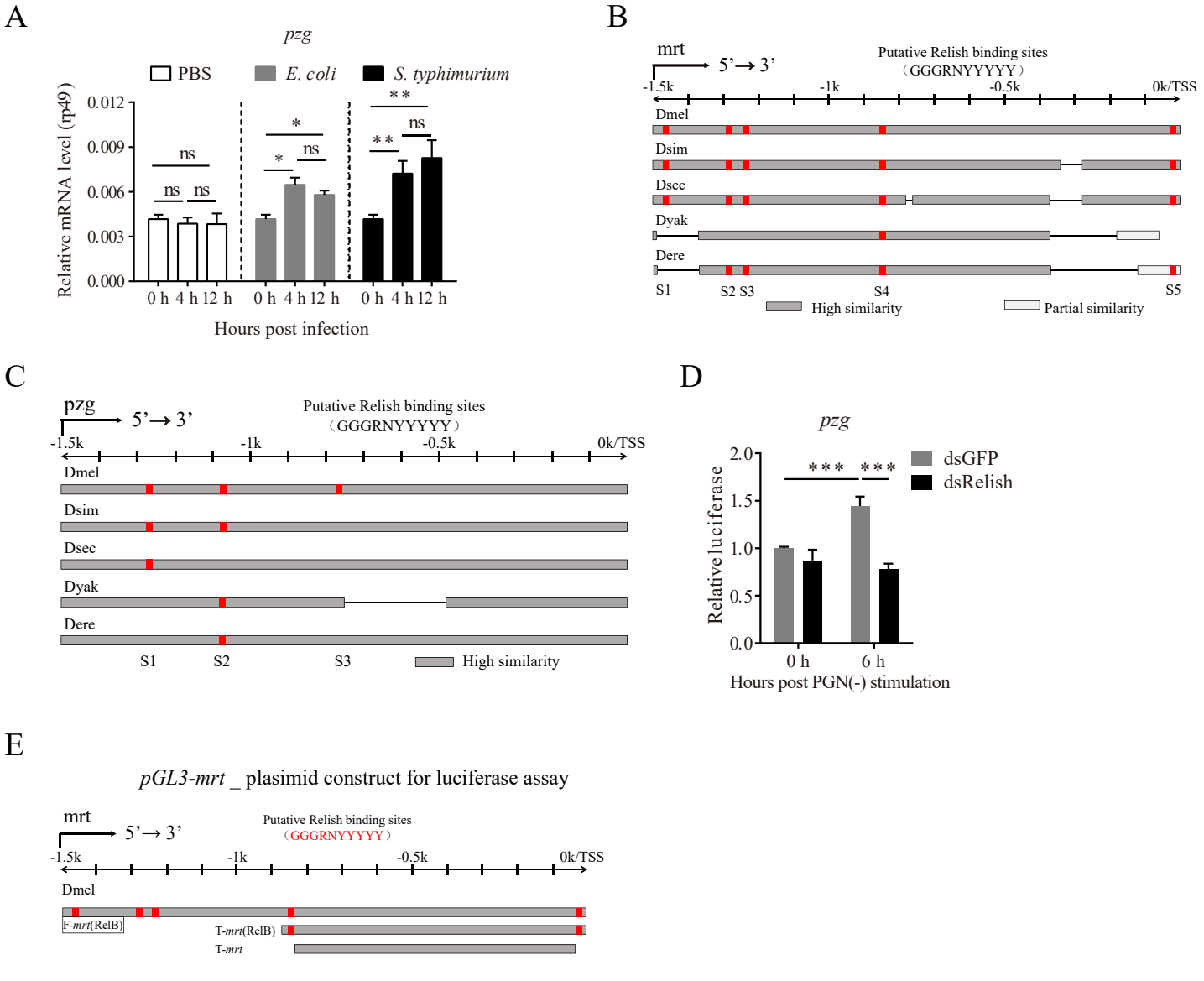
A
pzg
PBS
E. coli
S. typhimurium
Relative mRNA level (rp49)
0.012
0.009
0.006
0.003
0.000
ns
ns
ns
*
*
ns
**
**
ns
0 h 4 h 12 h
0 h 4 h 12 h
0 h 4 h 12 h
Hours post infection
B
mrt
5'→ 3'
Putative Relish binding sites
(GGGRNYYYYY)
-1.5k
-1k
-0.5k
0k/TSS
Dmel
Dsim
Dsec
Dyak
Dere
S1
S2 S3
S4
S5
High similarity
Partial similarity
C
pzg
5'→ 3'
Putative Relish binding sites
(GGGRNYYYYY)
-1.5k
-1k
-0.5k
0k/TSS
Dmel
Dsim
Dsec
Dyak
Dere
S1
S2
S3
High similarity
D
pzg
Relative luciferase
2.0
1.5
1.0
0.5
0.0
***
***
dsGFP
dsRelish
0 h
6 h
Hours post PGN(-) stimulation
E
pGL3-mrt _ plasimid construct for luciferase assay
mrt
5'→ 3'
Putative Relish binding sites
(GGGRNYYYYY)
-1.5k
-1k
-0.5k
0k/TSS
Dmel
F-mrt(RelB)
T-mrt(RelB)
T-mrt

Fig. S3. Relish/NF-κB potentially regulates the transcription of *mrt* or *pzg* in *Drosophila* subgroups. Related to Figure 2. (**A**) Relative *pzg* mRNA levels in the fat body of wild type flies post *E. coli* or *S. typhimurium* infection. Flies treated with sterile PBS were used as a control. The fold change of mRNA expression was normalized to that of 0 h. Four independent repeats (n=20 flies fat body tissues per repeat) were performed at each time point for each group. (**B and C**) Predicted Relish/NF-κB-binding motifs in the promoter locus of *mrt* (**B**) and *pzg* (**C**) genes of five *Drosophila* subgroups. Dmel, *Drosophila melanogaster*; Dsim, *D. simulans*; sec, *D. sechelia*; Dyak, *D. yakuba*; Dere, *D. erecta*. S1-S5 represent the location site (red color) of conserved binding motifs. Sequence alignment is analyzed by BLAST in flybase website. TSS: transcription start site. (**D**) Relative luciferase activities of *pzg* (1.5 KB upstream of ATG, all predicted Relish binding sites are covered) reporter in S2* cells after double strand RNA (dsRNA) and PGN (35 μg/ml) treatment. All data were normalized to dsGFP control group at 0 h. Three independent repeats were performed at each time point for each treatment. (**E**) Schematic diagram of the *mrt* promoter locus and the plasmid constructs used for luciferase assay. The full length (F-*mrt*(RelB):-1.5k to +1bp), truncated length (T-*mrt*(RelB):-870 to +1bp) and mutant length (T-*mrt*:-870 to +1bp without binding motifs) of *mrt* promoter were indicated. Error bars represent the mean ± s.d.. Data were analyzed by One-way ANOVA with Tukey's multiple-comparison test (**A**) and Student's t test (**D**). $^*p < 0.05$; $^{**}p < 0.01$; $^{***}p < 0.001$; ns, no significance.

Figure S4

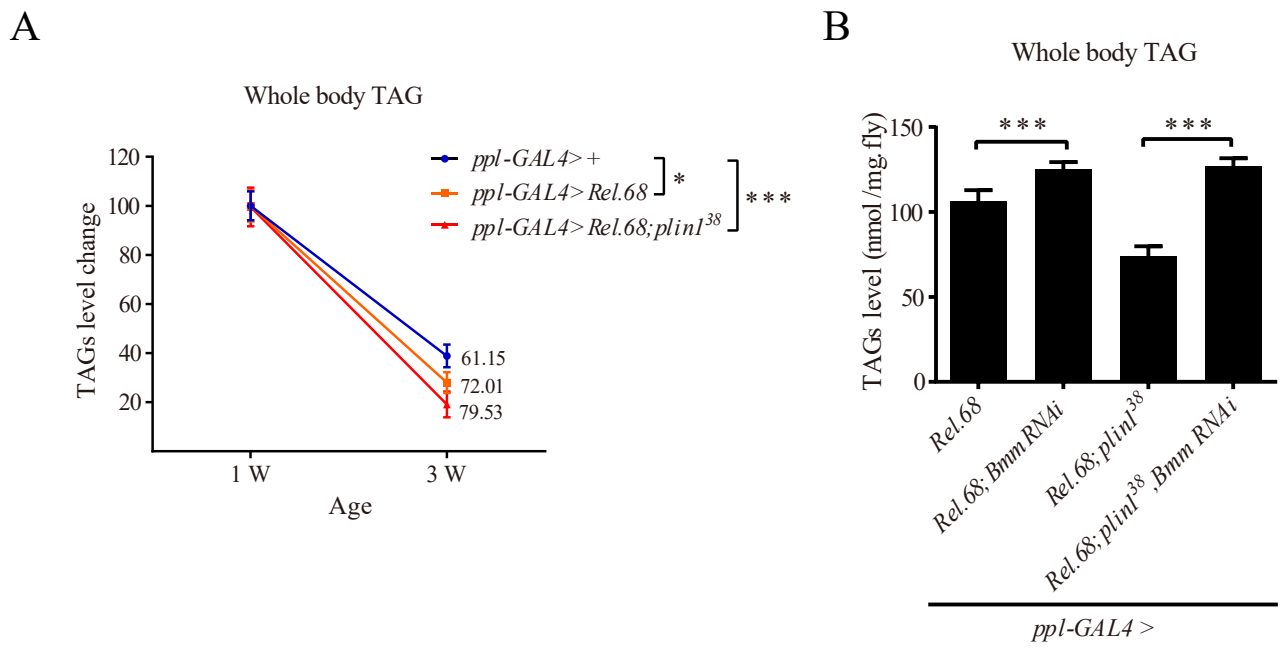
A
Whole body TAG
TAGs level change
120
100
80
60
40
20
ppl-GAL4> +
ppl-GAL4> Rel.68
ppl-GAL4> Rel.68;plin1^38
*
***
61.15
72.01
79.53
1 W
3 W
Age
B
Whole body TAG
TAGs level (nmol /mg fly)
150
100
50
0
***
***
Rel.68
Rel.68; Bmm RNAi
Rel.68; plin1^38
Rel.68; plin1^38 ;Bmm RNAi
ppl-GAL4 >

Fig. S4. *plin1* deficiency enhances Bmm/ATGL-dependent lipolysis in the condition of sustained IMD activation. Related to Figure 3. (**A**) TAGs level change in the whole body of indicated one-week or three-week old flies. The change of TAG levels at 3 w was normalized to that of 1w for each genotype. The number on the right of each line represents the percentage reduction of TAGs level at 3 w compared with 1 w for each genotype. Six independent replicates at each time point for each genotype were performed (n =12 flies per replicate). (**B**) Relative TAGs levels in the whole body of indicated one-week old adult flies. All values of TAGs level were normalized to that of 0h of *ppl-GAL4*>+ control flies. Six independent replicates for each genotype were performed (n =12 flies per replicate). Error bars represent the mean ± s.d.. Data were analyzed by One-way ANOVA with Student t-test. $^{*}p < 0.05$; $^{***}p < 0.001$.

Figure S5

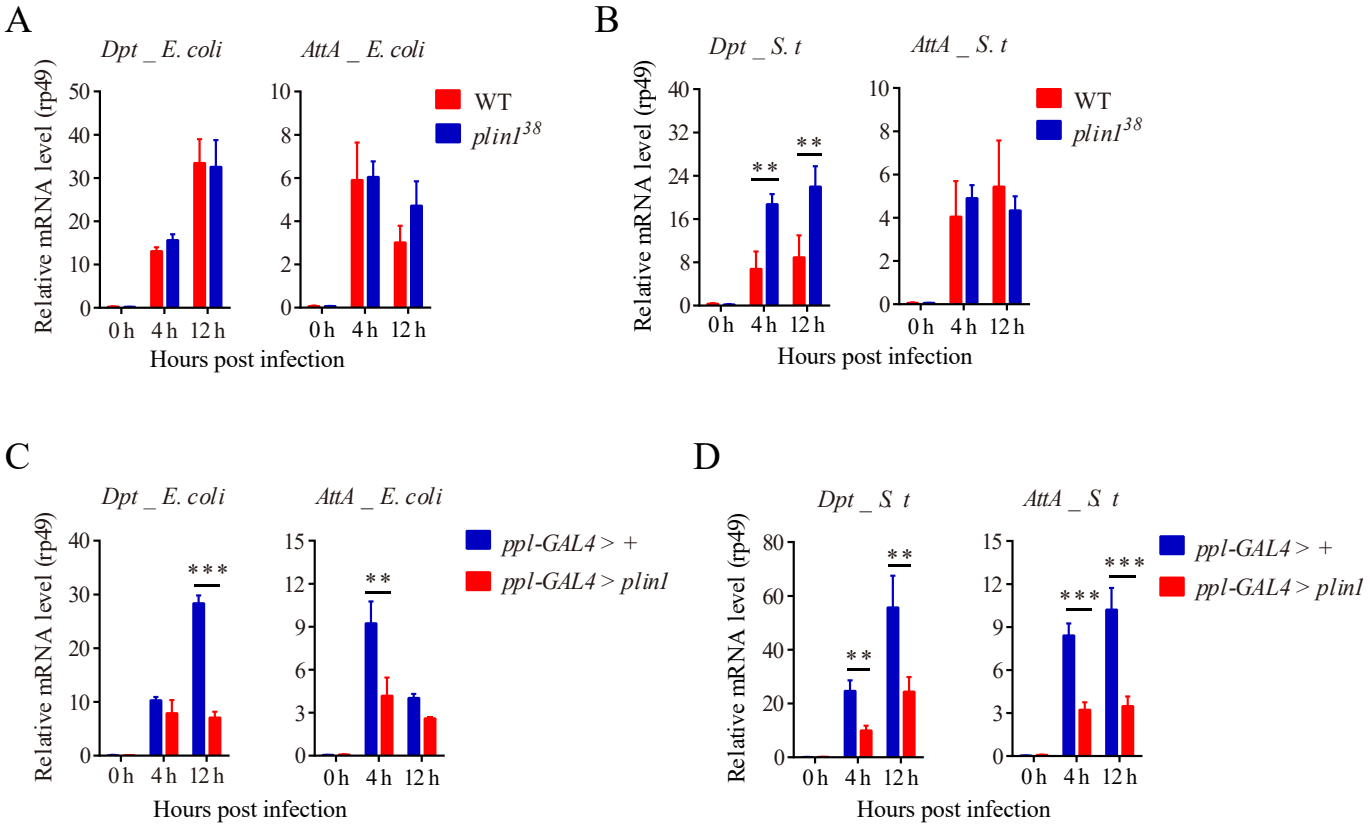
A
Dpt _ E. coli
AttA _ E. coli
Relative mRNA level (rp49)
WT
plin1^38
0 h
4 h
12 h
Hours post infection
B
Dpt _ S. t
AttA _ S. t
Relative mRNA level (rp49)
WT
plin1^38
**
**
Hours post infection
C
Dpt _ E. coli
AttA _ E. coli
Relative mRNA level (rp49)
ppl-GAL4 > +
ppl-GAL4 > plin1
***
**
Hours post infection
D
Dpt _ S. t
AttA _ S. t
Relative mRNA level (rp49)
ppl-GAL4 > +
ppl-GAL4 > plin1
**
**
***
***
Hours post infection

1222 **Fig. S5.** Overexpression *plin1* compromises AMP responses. Related to Figure 4. (**A**
1223 and **B**) Relative *diptericin (Dpt)* and *attacin-A (AttA)* mRNA expression in the fat body
1224 of $plin1^{38}$ mutant flies and wild type flies at indicated time points post *E. coli* (**A**) or *S.*
1225 *typhimurium* (**B**) infection. Four independent repeats were performed (n = 20 per
1226 repeat). (**C** and **D**) Relative *diptericin (Dpt)* and *attacin-A (AttA)* mRNA expression of
1227 *ppl-GAL4> plin1* flies and *ppl-GAL4>* + control flies at indicated time points post *E.*
1228 *coli* (**C**) and *S. typhimurium* (**D**) infection. Four independent repeats were performed (n
1229 = 20 per repeat). Error bars represent mean ± s.d. Data was analyzed by Multiple t-tests.
1230 $^{**}p < 0.01$; $^{***}p < 0.001$.
1231
1232
1233
1234
1235
1236
1237
1238
1239
1240
1241
1242
1243
1244
1245
1246
1247
1248
1249
1250
1251
1252
1253
1254
1255
1256
1257
1258
1259
1260
1261
1262
1263
1264
1265

1266 **Table S1: Primers used in this study.**

Genes	Forward primer	Reverse primer
	qRT-PCR primers	
Rp49	AGATCGTGAAGAAGCGCACCAAG	CACCAGGAACTTCTTGAATCCGG
Dpt	GGCTTATCCGATGCCCGACG	TCTGTAGGTGTAGGTGCTTCCC
AttA	CACAACTGGCGGAACTTTGG	AAACATCCTTCACTCCGGGC
plin1	CAGCGCATACCACTGGTCTAT	GCATTACCGATTTGCTTGACAG
plin2	CGAGCGCCTCCTTGAATAC	AGAACTCTTGCCATTCTGCAC
DGAT2/CG1942	GATTACTTTCCCGTGGAGCTGG	CCCATGTTAATGCCAATGCCTG
DGAT1/mdy	AAGACAGGCCTCTACTATTGT	CCCATCATGCCCATAAATGCC
DGAT/CG1941	GTTGCTGCCGTGCTGTTCTAT	GTGGGTTCTCTTGTGATTCGC
DGAT/CG1946	CTTCTTTACGCTGCCCATCTCG	CCATTACCTTCCATAATGCCG
GPAT1/CG5508	CCTTTTGGCCTTCACTTCC	TCTCGATCTGCTTCGTGTTC
APGAT4/CG4753	CTTCACATGCGGATTCTTCGTC	ACCATTCCGCCACACAGACAAG
APGAT3/CG4729	CTCTGTCCTGCATTTTCTACTACG	CTTGCTGATCTGCGTCTTGTTG
APGAT2/CG3812	GCTGGCCTAATCTTCATCG	CCCACAGTTTGATACGTTGC
APGAT1/CG17608	CTGTGCGTGCCCTTTATGATTC	CAGACCACGAACCTCCATTG
Lipin	GACATCCGCGATCTGTTTCCC	GGACTGGAATGTTTGGGTCAGC
Lip4	GACCGAACAAGGGACTTGG	CGAGTACGTATTGCCACGAA
ACC	GGAACACTGAACTGGGGAAA	GCAATCACGCTGGAGTTGTA
FASN	CGAATCCATCAATATGCCCG	ACATAGTGACCACCACCCAGGT
ACSL	TTCCGGCAAGATTATGCGTC	CAGTTGCTCCACAATTTGCTCA
dHSL	TTGCCCTCTTCAATGACAATCTG	CTGGTGGGTGTCCTTTCCA
BMM	AAGTATGCACCGCATCTGTTG	CAAATCGCAGAGGAGACAGC
sws/CG2212	CTGGATGGCGGCTATGTGAATAA	CCATTTCTTGTAGAGCAGCCAC
Cct1	TCCACCTCGCAGCAATTCTTC	GTAGTCACATCTATCCCGCTCC
Fatp	GAAATCCTTCTCGCGAATTCCT	GGAGATGAAAGCCATATCGCC
Rfabg	GGTTTCTGGCATATTGTTGA	TAGGGTGCGTATGCC ATCAA
DUOX	GCTGCACGCCAACCACAAGAGACT	CACGCGCAGCAGGATGTAAGGTTT
mrt	GGAGGATATTCTCGGAGTGGAGC	GCTTCCTGCCTCGTAGTCGAAC
pzg	GCTGAGGAACCACAACCATCTGAC	GTAACCTCGCCTTCGCCAGATT
	Primers for plasmid construction and dsRNA synthesis	
F-*mrt*(RelB)-luc	CGAGATCTGCGATCTAAGTATAACG TCGTAGCGCACACGCACACC	CAGTACCGGAATGCCAAGCTGGGT GCACCCTTTGATCAAGGTCTT
pzg-luc	CGAGATCTGCGATCTAAGTACACAG TAGCAGCACAACGGAGACG	CAGTACCGGAATGCCAAGCTCTGT AGCAGTTCTCGACGGACGCGT
T-*mrt*(RelB)-luc	CGAGATCTGCGATCTAAGTAGCCAC TTTGTCGCAGTGTATCTGT	CAACAGTACCGGAATGCCAGCTGG GTGCACCCTTTGATCAAG
T-*mrt*-luc	CGAGATCTGCGATCTAAGTACGTTA GCTTTTTGCTGTCATTCGT	CCAACAGTACCGGAATGCCAGATG CTGTTGGAAAACAAGCAA
dsRelish	TAATACGACTCACTATAGGGAGATC AAACACGTGCCGC	TAATACGACTCACTATACCCAGACT CACGCTCTGTCTC
dsGFP	TAATACGACTCACTATAGGGAGAAT GGTGAGCAAGGGCGAGGA	TAATACGACTCACTATAGGGAGACT TGTACAGCTCGTCCATGC

Supplementary Information for

Adaptive modification of lipid droplets mediated by Plin1 functions in infection-induced pathogenesis in *Drosophila*

Lei Wang[1,2,5], Jiaxin Lin[2,3,5], Junjing Yu[4], Zhiqin Fan[2,3], Hong Tang[2 #] and Lei Pan[2,3,6 #]

[1] Wuhan Institute of Virology, Chinese Academy of Sciences, Wuhan, Hubei 430071, China

[2] Key Laboratory of Molecular Virology and Immunology, Institut Pasteur of Shanghai, Chinese Academy of Sciences, Shanghai 200031, China

[3] CAS Center for Excellence in Biotic Interactions, University of Chinese Academy of Sciences, Beijing 100049, China

[4] Shanghai Institute of Biochemistry and Cell Biology, Chinese Academy of Sciences, Shanghai 200031, China.

[5] University of Chinese Academy of Sciences, Beijing 100049, China

[6] Lead contact

#Correspondence: H. Tang (htang@ips.ac.cn) or L. Pan (panlei@ips.ac.cn).

This PDF file includes:
SI Materials and Methods
Fig. S1 to S5 legend.
Table S1.

SI Materials and Methods.

Drosophila stocks and bacterial strain.

All flies were propagated at 25˚C on standard cornmeal food (1 L food contains 77.7 g cornmeal, 32.19 g yeast, 10.6 g agar, 0.726 g CaCl2, 31.62 g sucrose,63.2 g glucose, 2 g potassium sorbate and 15 ml 5% Tegosept),30%-55% humidity with a 12h/12h light/dark cycle. Fly resources that were used in this study as follows: w^{1118} were used as wild-type controls if no additional indication. *plin1*^{38}, *UAS-plin1* mcherry, *UAS-plin1 RNAi*, *Bmm-GFP* knock-in and *ppl-GAL4* were kindly gifted from Dr. Xun Huang (Institute of Genetics and Developmental Biology, CAS). *UAS-gstD-GFP* was kindly gifted from Dr. ZhiWei Liu (Shanghai Ocean University). w^{1118}*;P{GD5139=UAS-Bmm RNAi }*(VDRC, V37877 and V37880) were kindly gifted from Dr. Yong Liu (College of Life Sciences, Wuhan University). w^{1118}, *w[1118];P{w[+mW.hs]=Switch1}106*, *Bmm*^{1}, *w[*];P{w[+mC]=UAS-FLAG-Rel.68}i21-B; TM2/TM6C, Sb[1]*, *y[1] w[*]; P{w[+mC]=UAS-PGRP-LC.x}1* and *y[1] w[*]; P{w[+mC]=UAS-PGRP-LC.a}3* were obtained from Bloomington stock center. *UAS-PGRP-LC.x* and *UAS-PGRP-LC.a* were back-crossed to the w^{1118} flies for more than three generations prior to use. All flies used in this study were male. Two bacterial strain, *E. coli* (*DH5a*) and *S. typhimurium (SR-11)* (a gift from Dr. ZhiHua Liu, Institute of Biophysics, CAS) were used in this study.

Cloning and double-strand RNAs

To construct the *mrt* and *pzg* reporter vector (*mrt*-luc and *pzg*-luc), the *mrt* and *pzg* promoter sequence (about -1500 bp or -1000 bp to 0 bp) was PCR amplified from Drosophila genomic DNA and introduced into *pGL3* vector (Progema) at HindIII restriction site by using recombination technology (Hieff Clone® Plus One Step Cloning Kit, YEASEN). All the plasmid constructs were verified by nucleotide sequencing. *pAC5.1*-renilla plasmid as a normalized reporter. Double-stranded RNAs (dsRNAs) against relish or GFP used in the luciferase reporter assay were synthesized using MEGAscript T7 kit (Invitrogen). Primers used for PCR amplification are listed in Supplementary Table 1.

Infection and survival rate counting

Bacterial strains used in this study are *E. coli* (*DH5a*) and *Salmonella typhimurium* (*S. typhimurium*). Two days before infection, both bacteria from glycerol stocks were streaked onto Luria Broth (LB) agar plates and grown overnight at 37℃. The plate could be stored at 4 °C for up to 1 week. A single colony was inoculated to 6 ml fresh LB medium and grown at 37°C with shaking (200 rpm). Grow the bacteria to an OD600 of 0.7 to 0.8 (about 3.5 hours). The bacterial culture was pelleted with sterile phosphate-buffered saline (PBS) to the desired concentration. We injected 50.6 nl of bacterial suspension into dorsal prothorax of each fly with Nanoject II injector (Drummond). All flies used were 1 week old after eclosion. The final optical density (O.D. / ml) at 600 nm for injection were *E. coli* (O.D. 10) and *S. typhimurium* (O.D. 6 or O.D. 3). For *E.coli* infection, each fly obtained about 1x10^6 CFUs. For *S. typhimurium* infection, each fly obtained the lower dose (about 2x10^5 CFUs) or the higher dose (about 1x10^6 CFUs) according to the experiment design. Infected flies about 23 per vial were

maintained at 25°C. Death was recorded at the indicated time point, and alive flies were transferred to fresh food every day for the survival analysis and CFUs assay.

Lifespan counting

For lifespan analysis, male flies were collected within three days after adult emergence and raised in incubator (temperature: 25℃, humidity: 55%, 12:12 light: dark cycle). These flies were randomly divided into a separate vial in a number of 25 with at least three biological replicates. Dead flies were counted every three days and alive flies were flipped to fresh food.

Bacterial loads assay

To monitor bacterial loads of the flies during infection, the number of colony forming units (CFUs) grown on LB agar plate was determined as follow: 5 living flies were randomly collected in a 1.5 ml EP tube, rinsed with 70% ethanol two times by vertex for 10s to sterile the surface adherent bacteria, then rinsed with sterile deionized water two times by vertex for 10 s, and then homogenized in 200 µl of sterile PBS with three fly body volumes of ceramic beads (diameter: 0.5 mm) in the Minilys apparatus (Bertin TECHNOLOGIES) at highest speed for 30 s. The suspensions obtained were then serially diluted in PBS and plated on LB agar. Specially noted for S. typhimurium plating, PBS was substituted with PBS + 1% Triton X-100. For the bacterial load at zero time point, flies were allowed to rest for 10 min after bacterial injection before plating as described above. The agar plate was maintained at 37℃ for 18 hours before CFUs counting. CFUs were $\log_{10}$ transformed.

Cell culture, transfection and luciferase assay

S2* cells (a gift from Dahua Chen, Institute of Zoology, CAS) were maintained in Drosophila Schneider's Medium (Invitrogen) supplemented with 10% heat-inactivated fetal bovine serum (Gibco), 100 units/ml of penicillin, and 100 mg/ml of streptomycin at 28°C. Transient transfection of various plasmids, dsRNA was performed with lipofectamine 3000 (Invitrogen), according to the manufacturer's manual. Luciferase reporter assays were carried out using a dual-luciferase reporter assay system (Promega). Where indicated, cells were treated with PGN (35 µg/µl, 6 h) purified from Erwinia carotovora carotovora 15 (*Ecc15*) referring to previous study(1).

qRT-PCR

For quantification of mRNA level, about 20 flies carcass/fat body tissue were dissected in sterile PBS buffer on ice at indicated time points post infection, immediately homogenized in 200 µl cold TRIzol with three fly body volumes of ceramic beads (diameter: 0.5 mm), then supplied additional 300 µl TRIzol to reach total 500 µl volume and samples were stored at -80℃.RNA extraction was referred to the manual of commercial kit (Magen, Hipure Total RAN Plus Micro Kit), this kit can effectively remove genomic DNA contamination. cDNA was synthesized by using the kit (abm, 5X All-In-One MasterMix) with total 1µg isolated RNA as template in a 20 µl reaction system. Quantitative real-time PCR (qRT-PCR) was performed using a SYBR green kit

(abm, EvaGreen supermaster Mix) on an ABI 7500 or ViiATM 7 thermocycler (Life Technology). Samples from at least four independent biological replicates per genotype were collected and analyzed. House-keeping gene rp49 as the reference gene for data normalization. Primer data for qRT-PCR are provided in Supplementary Table 1.

Lipid droplet staining and counting

For lipid droplet staining, adult male carcass/fat body tissues were dissected and fixed in 4% fresh prepared paraformaldehyde (PH=7.5) in PBS for 10 min on ice. Tissues were then rinsed twice with PBS (3 min each time), then incubated in PBS containing 1μg/ml of BODIPY 493/503(Invitrogen) dye or 0.5 μg/ml Nile Red (Sigma) for 30 min on ice, DAPI (1μg/μl, final concentration) was added to stain nuclei at last 5 mins of staining process. After staining, tissues were rinsed three times with PBS (3 mins each time), then mounted in mounting medium (Vector, H-1000) for microscopy analysis. To quantify the average lipid droplet size, the average diameter of the three largest lipid droplets per cell was measured generally, with the exception of *plin1* deficiency associated flies, we just measured their biggest lipid droplet in one cell (2). 30 fat body cells of each genotype fly randomly selected from eight confocal images were used to analysis the lipid droplet size. To count the size distribution of lipid droplets, the average percentage of the indicated size range of lipid droplets per cell from 30 fat body cells were determined by using the "Analyze Particles" tool embedded in ImageJ software (https://imagej.nih.gov/ij/).

TAG assay

TAG amounts were measured using a TG Quantification Kit (BIOSINO, TG kit). Briefly, for whole body TAG quantification, groups of 12 one-week old male flies were collected and weighted (about 10 mg) in a 1.5 ml EP tube, then immediately stored at -80°C for subsequent assay. Stored flies were homogenized in 200 μl lysis buffer (10mM KH_2PO4, 1mM EDTA, PH=7.4) with three fly body volumes of ceramic beads, and inactivated in water bath at 75°C for 15 min. The inactivated homogenate was homogenized again for 30 s and kept on ice ready for assay. For each TAG measurement, 3 μl of homogenate was incubated with 250 μl reaction buffer at 37°C for 10 min. After removal debris by centrifugation (2000 rpm, 2 min), 150 μl of clear supernatant was used to perform a colorimetric assay in 96 well plate (Corning® Costar) for absorbance reading at 505 nm. TAGs level was normalized with fly weight in each homogenate (unit: nmol/mg.fly). For fat body TAG quantification, 25 fly's carcass/fat body tissues were dissected and following assay as described above. TAGs level was normalized with per 25 flies (unit: nmol/25.fly).

RU486 treatment

RU486 induction was described as before (3). Briefly, A 10 mg/ml stock solution of RU486 (mifepristone; Sigma) was dissolved in DMSO. Appropriate volumes of RU486 stock solution was diluted with water containing 2% ethanol to final concentration of 50 μg/ml.100 μl of the diluted RU486 solution was dipped onto the surface of fresh food in vials (Diameter: 2 cm). The vials were then allowed to dry at room temperature

for half day or 4℃ for overnight. Flies were transferred to RU486-contained food and raised in 25℃ and fresh food was changed every two days.

NAC Treatment

N-acetyl-L-cysteine (NAC) (Beyotime) fresh solution was prepared by dissolving 0.5 g of NAC powder in 10 ml distilled water, the solution could be aliquoted into 1 ml per EP tube and frozen or stored at -80 °C. 100 μl of NAC solution was dipped onto the surface of fresh food in vials (Diameter: 2 cm). The vials were then allowed to dry at room temperature for half day or 4℃ for overnight. Flies were transferred to NAC-contained food and raised in 25℃ and fresh food was changed every day.

ROS detection

We used two methods to detect ROS in fat body, which are *gstD-GFP* reporter flies and dichlorofluorescein diacetate (DCFH-DA) labeling. The oxidative stress reporter construct *gstD-GFP* for evaluating cellular ROS levels has been describe before (4). Briefly, the carcass/fat body of transgenic flies containing a *gstD-GFP* reporter construct were dissected in sterile PBS, fixed in 4% formaldehyde for 10 min on ice, rinsed twice with ice-chilled PBS (3 min each time), then the flaky fat body cells attached to the inner carcass shell were dissected out to mount and confocal image (Vector, H-1000). DCFH-DA (Beyotime, Reactive Oxygen Species Assay Kit) labeling of fresh dissected carcass/fat body tissues was performed according to the manufacturer's manual, which based on the ROS-dependent oxidation of DCFH-DA to fluorescent molecule 2-7dichlorofluorescein (DCF). In brief, the tissues were incubated with PBS containing 20 μM DCFH-DA for 30 min at 37℃, washed with sterile PBS for three times (3 min each) to remove free DCFH-DA that do not uptake by the cell, then the flaky fat body cells attached to the inner carcass shell immediately were dissected out to mount and confocal image (Vector, H-1000). It should be noted that the slices were confocal imaged using the exact same settings for control and experimental groups. The fluorescence intensity is proportional to the ROS levels, fluorescence intensity of GFP or DCF was quantified by using ImageJ software.

Starvation test

Adult male flies were collected within three days after eclosion and raised on standard fly food at 25˚C. One week later, flies were randomly distributed in groups of 20 flies/vial and starved on 1% agar (dissolved in distilled water), new agar vial was changed every day. For the survival counting, the deaths were scored every two hours until all experimental files were dead. For the TAG assay, 12 alive flies were randomly collected at indicated time point, and delivered to TAG assay as describe above.

Microscopy and software

LSM700 (Leica) and Olympus FV-1200 confocal laser scanning microscopy were used for imaging. Captured images were analyzed by implemented soft respectively. ImageJ (https://imagej.nih.gov/ij/) was used for analysis of fluorescence intensity and lipid droplets size.

Statistical analyses

All replicates are showed as the mean ± SD or mean with range. Statistical significance was determined using a paired Student's t-test for two measurements, one-way ANOVA (Tukeys HSD) with a multiple t -tests and Multiple t-tests for pairwise comparisons. Kaplan–Meier test for survival curves comparison. All data processing was used with GraphPad Prism 7.0.

Supplementary Figure Legends

References for SI

1. Gottar M GV, Michel T, Belvin M, Duyk G, Hoffmann JA, Ferrandon D, Royet J. (2002) The Drosophila immune response against Gram-negative bacteria is mediated by a peptidoglycan recognition protein. *Nature* 11(416(6881)):640-644.
2. Bi J*, et al.* (2012) Opposite and redundant roles of the two Drosophila perilipins in lipid mobilization. *Journal of cell science* 125(Pt 15):3568-3577.
3. Poirier L SA, Zheng J, Seroude L. (2008) Characterization of the Drosophila gene-switch system in aging studies: a cautionary tale. *Aging Cell. 2008 Oct;* 7(5)(758-70.).
4. Sykiotis GP & Bohmann D (2008) Keap1/Nrf2 signaling regulates oxidative stress tolerance and lifespan in Drosophila. *Developmental cell* 14(1):76-85.